

NASA CR 125072

THE UNIVERSITY OF MICHIGAN
ANN ARBOR, MICHIGAN

SEMIANNUAL PROGRESS REPORT NO. 10

ON

MICROWAVE DEVICE INVESTIGATIONS


This report covers the period April 1, 1971 to October 1, 1971

**CASE FILE
COPY**

Electron Physics Laboratory
Department of Electrical and Computer Engineering

By: G. I. Haddad
R. J. Lomax
N. A. Masnari
S. N. Shabde

Approved by:


G. I. Haddad, Director
Electron Physics Laboratory

Project 084000

RESEARCH GRANT NO. NGL 23-005-183
OFFICE OF SPACE SCIENCE AND APPLICATIONS
NATIONAL AERONAUTICS AND SPACE ADMINISTRATION
WASHINGTON, D. C. 20546

November, 1971

TABLE OF CONTENTS

	<u>Page</u>
1. GENERAL INTRODUCTION	1
2. NOISE MODULATION IN AVALANCHE-DIODE DEVICES	1
2.1 Introduction	1
2.2 Summary of Work Completed	2
2.2.1 Calculation of Noise Parameters	2
2.2.2 Measurement of Noise Figure	2
2.2.3 Corpuscular Model of Avalanche Noise	3
2.2.4 Effect of Fluctuations in Reverse Saturation Current	3
2.2.5 Study of Noise Reduction Methods	3
2.2.6 Injection Locking in Avalanche-Diode Oscillators	4
2.3 Program for the Next Period	4
3. SCHOTTKY-BARRIER MICROWAVE DEVICES (MINITT OR BARITT DEVICES)	5
3.1 Introduction	5
3.2 General Remarks	5
3.3 Fabrication of Ti-Si(p)-Ti Structures	9
3.4 Fabrication of PtSi-Si(n)-PtSi Structures	12
3.5 Experimental Study of I-V Characteristics of MINITT [PtSi-Si(n)-PtSi] Structures	12
3.6 Theoretical dc I-V Characteristic of the MINITT Structure	16
3.7 Program for the Next Period	18
4. INTERMODULATION PRODUCTS IN IMPATT DIODE AMPLIFIERS	19
4.1 Introduction	19
4.2 Test Setup	19
4.3 Single-Frequency Operation	19
4.4 Two-Frequency Operation	21
4.5 Conclusions	30
4.6 Program for the Next Period	33

	<u>Page</u>
5. HARMONIC GENERATION USING READ DIODE VARACTORS	33
5.1 Introduction	33
5.2 Power Output and Efficiency of a Read Diode Varactor	34
5.3 Experimental and Theoretical C-V Characteristics of Read Diode Varactors	42
5.4 Conclusions	42
5.5 Program for the Next Period	42
6. FABRICATION OF SCHOTTKY-BARRIER IMPATT DIODES	46
6.1 Introduction	46
6.2 Ti-Si(p) Schottky Barrier	46
6.2.1 Fabrication	46
6.2.2 Height of Ti-Si(p) Schottky Barrier	47
6.3 PtSi-Si(n) Schottky Barrier	51
6.4 Conclusions and Program for the Next Period	51

LIST OF ILLUSTRATIONS

<u>Figure</u>		<u>Page</u>
3.1	Open-Base MINITT Transistor.	6
3.2	A Double Schottky-Barrier Structure.	8
3.3	Schottky Barrier. ($\phi_{Bn1} \gg \phi_{Bn2}$)	10
3.4	Pulsed I-V Characteristics of Ti-Si(p)-Ti for Both Polarities.	11
3.5	Physical Structures of MINITT Devices on a Common Gold Base.	14
3.6	I-V Characteristics of MINITT Devices.	15
4.1	Two-Frequency Test Apparatus for an IMPATT Diode Reflection Amplifier.	20
4.2	Single-Frequency Gain Characteristic for an IMPATT Diode Reflection Amplifier.	22
4.3	Dynamic Characteristics of an IMPATT Diode Reflection Amplifier for Two Equal Amplitude Input Signals. ($\Delta f = 3$ MHz)	24
4.4	Dynamic Characteristics of an IMPATT Diode Reflection Amplifier for Two Equal Amplitude Input Signals. ($\Delta f = 10$ MHz)	26
4.5	Dynamic Characteristics of an IMPATT Diode Reflection Amplifier for Two Equal Amplitude Input Signals. ($\Delta f = 30$ MHz)	27
4.6	Dynamic Characteristics of an IMPATT Diode Reflection Amplifier for Two Equal Amplitude Input Signals. ($\Delta f = 100$ MHz)	29
4.7	Dynamic Characteristics of an IMPATT Diode Reflection Amplifier for Two Equal Amplitude Input Signals. ($\Delta f = 10$ MHz)	31
4.8	Dynamic Characteristics of an IMPATT Diode Reflection Amplifier for Two Equal Amplitude Input Signals. ($\Delta f = 30$ MHz)	32
5.1	C-V Characteristic of a Read Diode Varactor.	36
5.2	C-V Characteristic of an Ideal Punch-Through Varactor.	37

FigurePage

5.3	Theoretical Efficiency of the Read Diode Varactor of Fig. 5.1 for Different N_1 and N_2 Values. ($\gamma_1 = 0.5$, $\gamma_2 = 4$, $\bar{v}_{pt} = 0.2$, $\bar{v}'_{pt} = 0.3$, $\omega_{out}/\omega_c = 10^{-2}$)	38
5.4	Theoretical Normalized Power Output of the Read Diode Varactor of Fig. 5.1 for Different N_1 and N_2 Values. ($\gamma_1 = 0.5$, $\gamma_2 = 4$, $\bar{v}_{pt} = 0.2$, $\bar{v}'_{pt} = 0.3$, $\omega_{out}/\omega_c = 10^{-2}$)	39
5.5	Theoretical Efficiency of the Varactor of Fig. 5.2 for Different N_1 and N_2 Values. ($\gamma_1 = 0.5$, $\gamma_2 = 0$, $\bar{v}_{pt} = 0.2$, $\bar{v}'_{pt} = 0.2$, $\omega_{out}/\omega_c = 10^{-2}$)	40
5.6	Theoretical Normalized Power Output of the Varactor of Fig. 5.2 for Different N_1 and N_2 Values. ($\gamma_1 = 0.5$, $\gamma_2 = 0$, $\bar{v}_{pt} = 0.2$, $\bar{v}'_{pt} = 0.2$, $\omega_{out}/\omega_c = 10^{-2}$)	41
5.7	Theoretical C-V Curve of the TI Read Diode.	43
5.8	Experimental C-V Curve of the TI Read Diode.	44
5.9	Theoretical C-V Curve of a Read Diode with Different Doping Density in the i-Layer.	45
6.1	I-V Characteristics of the Ti-Si(p) Schottky Barrier.	48
6.2	C-V Characteristic of the Ti-Si(p) Schottky Barrier.	49
6.3	Breakdown Characteristic of a PtSi-Si(n) Schottky Barrier.	52

PUBLICATIONS DURING THE LAST PERIOD

C. Yeh and S. N. Shabde, "Temperature Dependence of Ionization Rates in $\text{Al}_x\text{Ga}_{1-x}\text{As}$," Solid-State Electronics, vol. 14, No. 7, pp. 557-562, July 1971.

M. S. Gupta and R. J. Lomax, "A Self-Consistent Large-Signal Analysis of a Read-Type IMPATT Diode Oscillator," IEEE Trans. on Electron Devices, vol. ED-18, No. 8, pp. 544-550, August 1971.

C. F. Krumm and G. I. Haddad, "Millimeter- and Submillimeter-Wave Detection by Paramagnetic Materials," IEEE J. of Quantum Electronics, vol. QE-7, No. 10, pp. 475-484, October 1971.

M. S. Gupta, "Noise in Avalanche Transit-Time Devices," Proc. IEEE, December 1971 (to be published).

S. P. Kwok and G. I. Haddad, "The Effects of Tunneling on an IMPATT Oscillator," J. Appl. Phys. (submitted for publication).

M. S. Gupta, "Avalanche Current Noise in Semiconductors Under Self-Sustaining Breakdown," Solid-State Electronics (submitted for publication).

S. P. Kwok and G. I. Haddad, "The Effects of Tunneling on an IMPATT Oscillator," Presented at the 1971 Device Research Conf., Ann Arbor, Mich., June 28-July 1, 1971.

M. S. Gupta and R. J. Lomax, "Injection Locking in IMPATT Diode Oscillators," Presented at the 1971 Cornell Conf. on High Frequency Generation and Amplification: Devices and Applications, Ithaca, N. Y., August 1971.

SEMIANNUAL PROGRESS REPORT NO. 10

ON

MICROWAVE DEVICE INVESTIGATIONS

1. General Introduction (G. I. Haddad)

The purpose of this program is to investigate materials, devices and novel schemes for generation, amplification and detection of microwave and millimeter-wave energy. Several tasks were active during this report period under this program. These include:

1. Noise modulation in avalanche-diode devices.
2. Schottky-barrier microwave devices.
3. Intermodulation products in IMPATT diode amplifiers.
4. Harmonic generation using Read-diode varactors.
5. Fabrication of GaAs Schottky-barrier IMPATT diodes.

The work performed on these tasks is described in detail in the following sections of this report.

2. Noise Modulation in Avalanche-Diode Devices

Supervisor: R. J. Lomax

Staff: M. S. Gupta

2.1 Introduction. The objectives of this phase of the program have been to study the noise behavior of avalanche-diode devices and to evaluate the methods available for noise reduction. The investigation has been concerned with both avalanche-diode amplifiers and oscillators. This work has now been terminated. A summary of the work carried out under this phase through June 1971 is included below.

2.2 Summary of Work Completed. Several problems were taken up for study under this phase of the program and the work on each of these is reviewed here. Most of the results of these investigations have been published.¹⁻⁴

2.2.1 Calculation of Noise Parameters. An algorithm was devised for the calculation of the four noise parameters of a linear two-port from experimental measurements of its noise figure as a function of the source admittance. A computer program for performing this calculation was written and a brief description of it has been published.¹ In particular, this program calculates the minimum noise figure of the two-port and the value of the corresponding source admittance.

2.2.2 Measurement of Noise Figure. The noise figure of a stable reflection-type (circulator coupled) coaxial-cavity X-band avalanche-diode amplifier, which has a small-signal gain of 12 dB, was measured using a noise figure meter and a gas discharge-type waveguide noise source. The noise figure was approximately 20 dB. This value is at one end of the noise figure range over which measurements could be carried out and therefore measurements of small changes in the noise figure were not reliable. More accurate results

-
1. Gupta, M. S., "Determination of the Noise Parameters of a Linear 2-Port," Electronics Letters, vol. 6, No. 17, pp. 543-544, 20 August 1971.
 2. Gupta, M. S., "Avalanche Current Noise in Semiconductors under Self-Sustaining Breakdown," Solid-State Electronics (submitted for publication).
 3. Gupta, M. S., "Noise in Avalanche Transit-Time Devices," Proc. IEEE, December 1971 (to be published).
 4. Gupta, M. S. and Lomax, R. J., "Injection Locking in IMPATT Diode Oscillators," Proc. Third Biennial Cornell Conf. on High-Frequency Generation and Amplification: Devices and Applications, Ithaca, N. Y., August 1971 (to be published).

would require an X-band noise source with greater output than was available.

2.2.3 Corpuscular Model of Avalanche Noise. The noise spectrum of an avalanche-generated current in a uniform semiconductor was found for a self-sustaining avalanche when the avalanche current contains a periodic signal component. The avalanche current was modeled as a periodically nonstationary random process by a pulse train of overlapping current pulses. The electron and hole ionization rates were assumed to be equal and the carrier velocities were assumed saturated and equal. The results² differ from the Schottky theorem generalized for a finite transit time because the model also takes into account the fact that two carriers are simultaneously generated and individual carriers have different transit times.

2.2.4 Effect of Fluctuations in Reverse Saturation Current.

It has been suggested by several authors that under large-signal conditions the conduction current minima of the avalanche diode are limited by the reverse saturation current I_s , and therefore the fluctuations in I_s which become amplified during the current buildup part of the cycle should have a strong influence on the total noise generation. The Schottky theorem does not appear to be applicable to I_s due to its very small value, so a carrier clustering effect in the small stream of carriers during current minima was postulated. The calculated noise spectrum of I_s shows that the presence of correlation reduces the magnitude of the noise.

2.2.5 Study of Noise Reduction Methods. An exhaustive study³ of reported results concerning noise in avalanche transit-time devices was made to find the optimum noise performance which is achievable from these devices and the methods that have been suggested for the minimization of noise. The scope of this study was very broad; it included examination

of both theoretical and experimental work on all modes of operation of these devices in several applications (noise generators, free-running and injection-locked oscillators, negative resistance and parametric amplifiers, and mixers).

2.2.6 Injection Locking in Avalanche-Diode Oscillators. Since injection locking is one of the most effective methods of reducing FM noise in avalanche-diode oscillators, a study was made to determine the utility and limitations of injection locking as a noise reduction technique for these oscillators. A model of an injection-locked avalanche-diode oscillator was devised. The model treats injection locking as the phenomenon of forced oscillations in a nonlinear oscillator. The device is represented by a nonlinear impedance (with a negative real part) which is a function of operating frequency and RF amplitude. The oscillator circuit is represented by a general network with frequency-dependent resistances and reactances. Both of these impedances are numerically determined on a digital computer: the diode impedance from a large-signal analysis, and the circuit impedance from an equivalent-network representation of a diode package and coaxial cavity. An iterative numerical procedure⁴ is used to compute the locking bandwidth as a function of locking gain, the change in the output power of the oscillator upon locking as a function of frequency separation between the free-running and locking signal frequencies, and the locking figure of merit as a function of the diode operating point.

2.3 Program for the Next Period. This work has been completed and its major findings have been published in four communications. No further work is planned under this phase of the program.

3. Schottky-Barrier Microwave Devices (MINITT or BARITT Devices)

Supervisor: G. I. Haddad

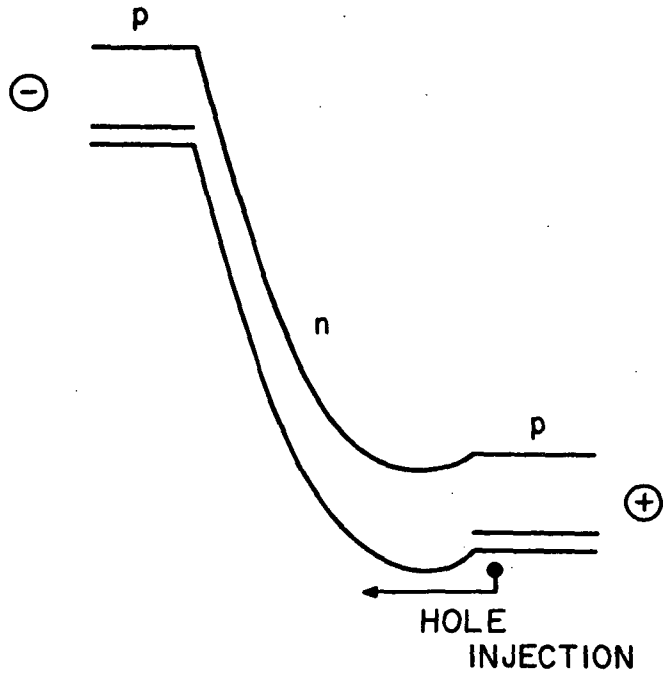
Staff: S. P. Kwok

3.1 Introduction. The MINITT or BARITT device was introduced recently¹ and shows a great deal of promise as a low-noise microwave device. During this period a general preliminary study of the device was made, the theoretical dc I-V characteristic was derived and fabrications of the device using Ti-Si(p)-Ti and PtSi-Si-PtSi were initiated.

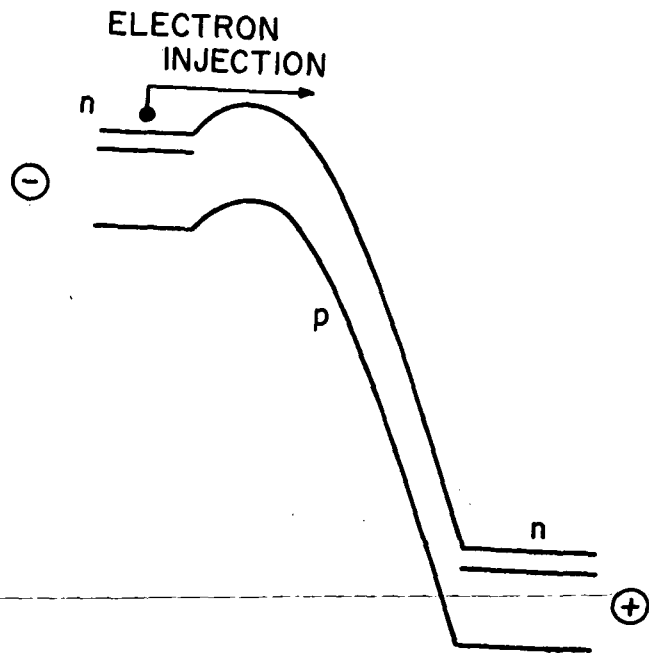
3.2 General Remarks. In general, the MINITT (minority carrier injection transit time) or BARITT (barrier injection transit time) structure consists of two back-to-back diodes joined by a narrow "base" region. Barrier injections could include either minority or majority carrier injection. The term majority carrier injection transit time will be abbreviated as MAJITT. The BARITT structures can then be classified in terms of MINITT, MAJITT or a combination of both. A wide variety of junction devices, such as open-base transistors, double Schottky barriers, metal p-p⁺ structures and even Schottky barriers can be classified as BARITT.

In Fig. 3.1 the band structures of complementary open-base transistors are given. If the injection efficiencies of the junctions are high, then such structures are always of the MINITT type. The current is small and equal to saturation current of the reverse biased p-n junction at voltages below the reach-through voltage. The reach-through voltage V_{RT} is given by

1. Coleman, D. J., Jr. and Sze, S. M., "A Low-Noise Metal-Semiconductor-Metal (MSM) Microwave Oscillator," Bell System Tech. J., vol. 50, No. 5, pp. 1695-1699, May-June 1971.



(a) pnp



(b) npn

FIG. 3.1 OPEN-BASE MINITT TRANSISTOR.

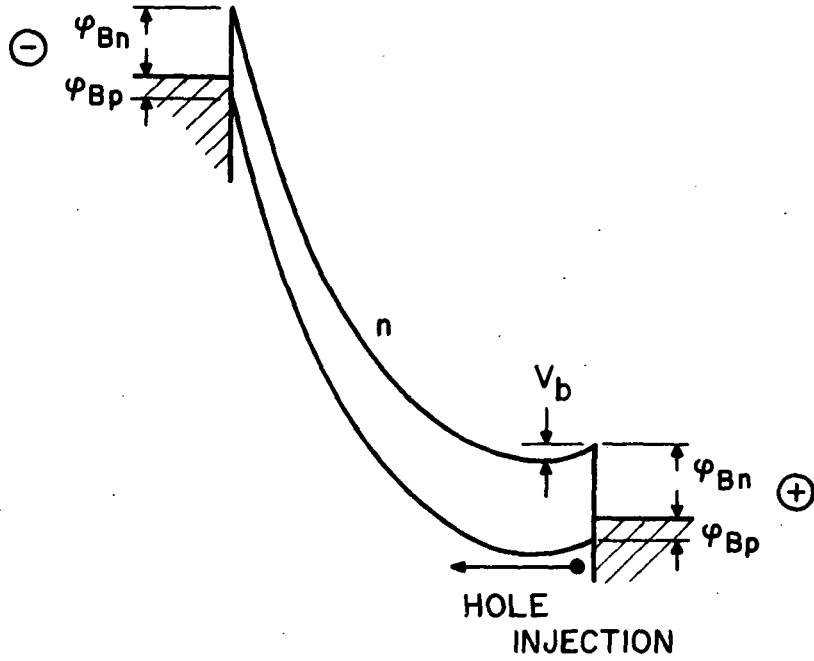
$$V_{RT} \cong \frac{q}{\epsilon} \frac{NL^2}{2}, \quad (3.1)$$

where q is the electronic charge, ϵ is the dielectric constant of the semiconductor, N is the doping density of the base which is assumed to be constant and L is the base width. If the voltage exceeds V_{RT} , significant minority carriers are injected causing a large increase in current.

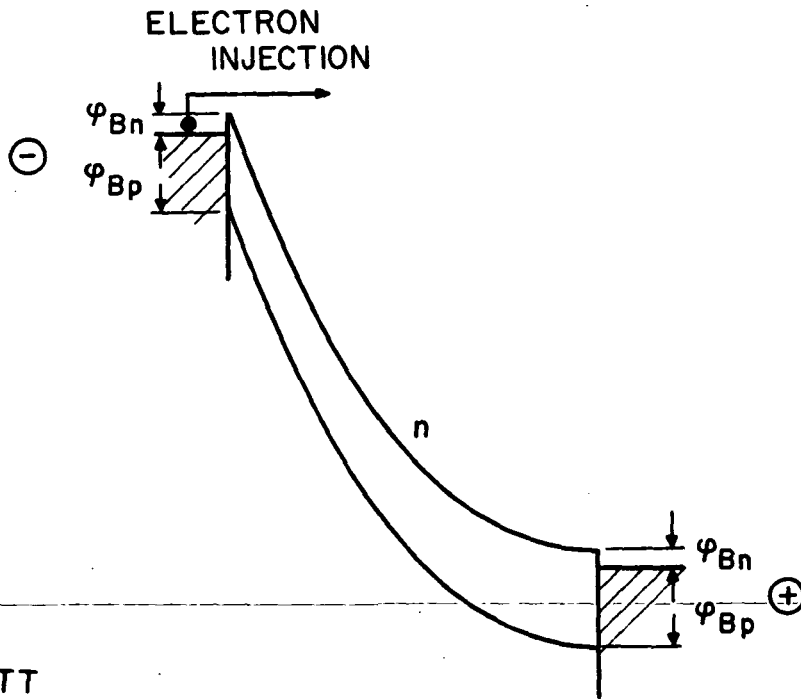
Figure 3.2a shows a double Schottky-barrier structure with a large barrier height, $\phi_{Bn} \gg \phi_{Bp}$. At the metal interface the quasi-Fermi level is assumed to be the same as that of the metal. Such an assumption implies that the injection of carriers does not perturb the electron thermal equilibrium population in the metal. The hole population p at the interface is given by

$$p = N_v \exp\left(-\frac{q\phi_{Bp}}{kT}\right), \quad (3.2)$$

where k is the Boltzmann constant, T is the temperature, q is the electronic charge and N_v is the effective density of states in the valence band. For a large $\phi_{Bn} = \mathcal{E}_q - \phi_{Bp}$, where \mathcal{E}_q is the bandgap, the hole population at the interface becomes large. These minority holes then are injected over a built-in barrier voltage V_b of the forward-biased junction. Moreover, a large barrier ϕ_{Bn} only allows a few electrons (majority carriers) to be injected from the left contact. Thus, this structure is of the MINITT type. Figure 3.2b shows the same structure as before except with a small barrier height, $\phi_{Bn} \ll \phi_{Bp}$. In this case there is an abundance of majority carriers (electrons) injected from the left barrier while few holes are injected from the right-hand side. Such a structure is a MAJITT. It is observed immediately that a MAJITT structure is relatively unimportant for microwave



(a) MINITT
 $\phi_{Bn} \gg \phi_{Bp}$



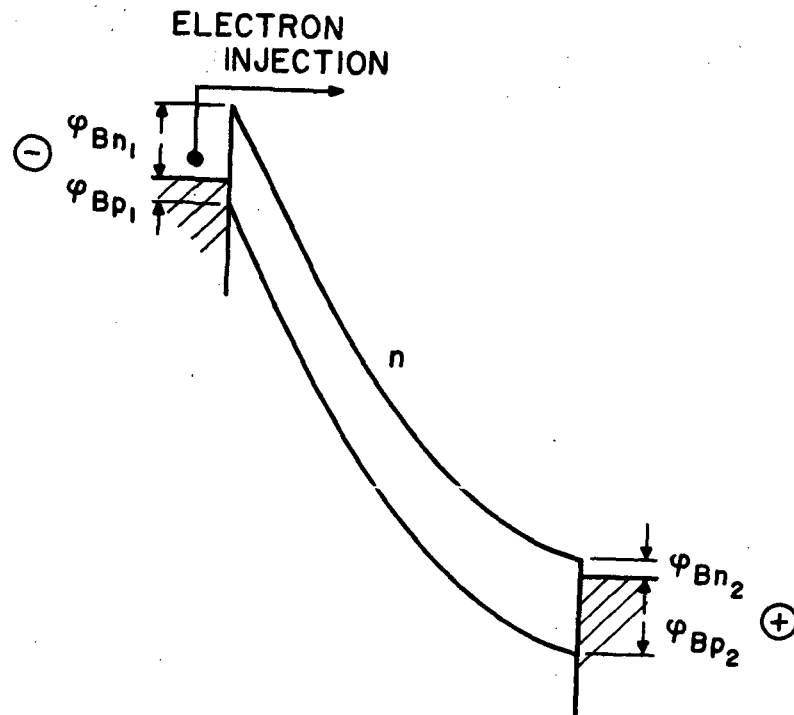
(b) MAJITT
 $\phi_{Bn} \ll \phi_{Bp}$

FIG. 3.2 A DOUBLE SCHOTTKY-BARRIER STRUCTURE.

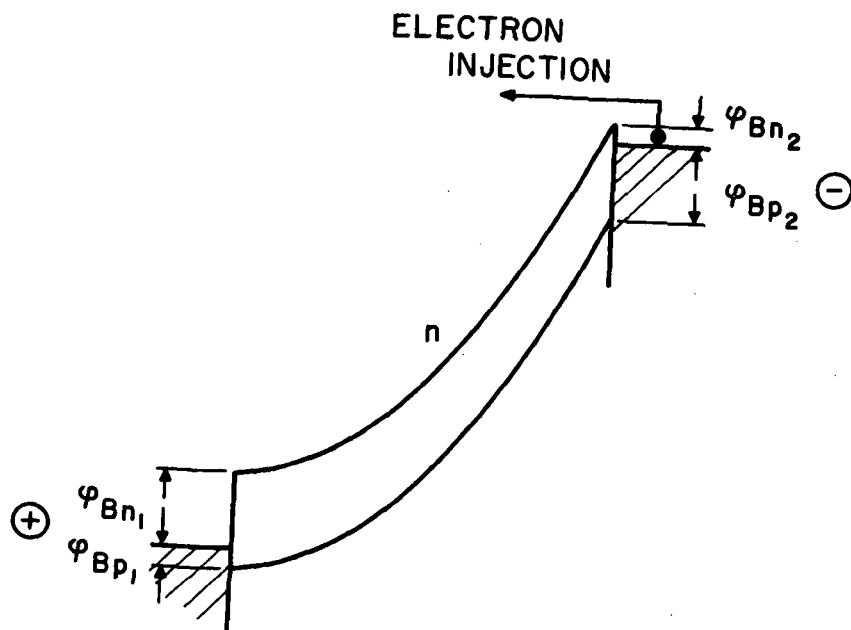
generation. This is because of the inherently large saturation current which also tends to introduce a thermal problem similar to that known as secondary breakdown of a transistor. In the case of barriers with intermediate heights, both minority and majority carrier injections are expected to take place. Besides the complications just mentioned, the problem is more complicated mathematically since it involves two types of carriers. This study will concentrate on the MINITT structure.

The band structures of a Schottky barrier under reverse and forward biases are given in Fig. 3.3. The ohmic contact is taken to be a barrier with a small height. There is little minority hole injection in such a barrier and any rapid rise in current in the reverse direction will be due to avalanche multiplication.

3.3 Fabrication of Ti-Si(p)-Ti Structures. A 50- Ω p-type Si slice was chemically thinned to about 10 μm . At such a thickness the wafer becomes light brown and is semitransparent. The cleaning process, the evaporations of metals and the diode separations are described in Section 6 of this report. After the evaporation of the metals the wafer is sintered in a nitrogen environment at 350°C for five minutes and the diodes are then separated and used for evaluation. The resultant I-V characteristic exhibits a hysteresis loop, similar to that of transistor secondary breakdown, on the curve tracer due to heating. The pulsed I-V characteristic of such a diode is asymmetrical as illustrated in Fig. 3.4. However, the diode punch through occurs between 56 V and 82 V, which is of the proper order of magnitude as the theoretical prediction ($V_{RT} = 40$ V for $N_D \approx 5 \times 10^{14}/\text{cm}^3$ and $L = 10 \mu\text{m}$). The negative resistance is due to thermal effects and is similar to the secondary breakdown of a transistor. The voltage at which the diode exhibits negative resistance decreases with increasing pulse width and reaches a minimum value under dc conditions.



(a) REVERSE BIASED



(b) FORWARD BIASED

FIG. 3.3 SCHOTTKY BARRIER. ($\phi_{Bn_1} \gg \phi_{Bn_2}$)

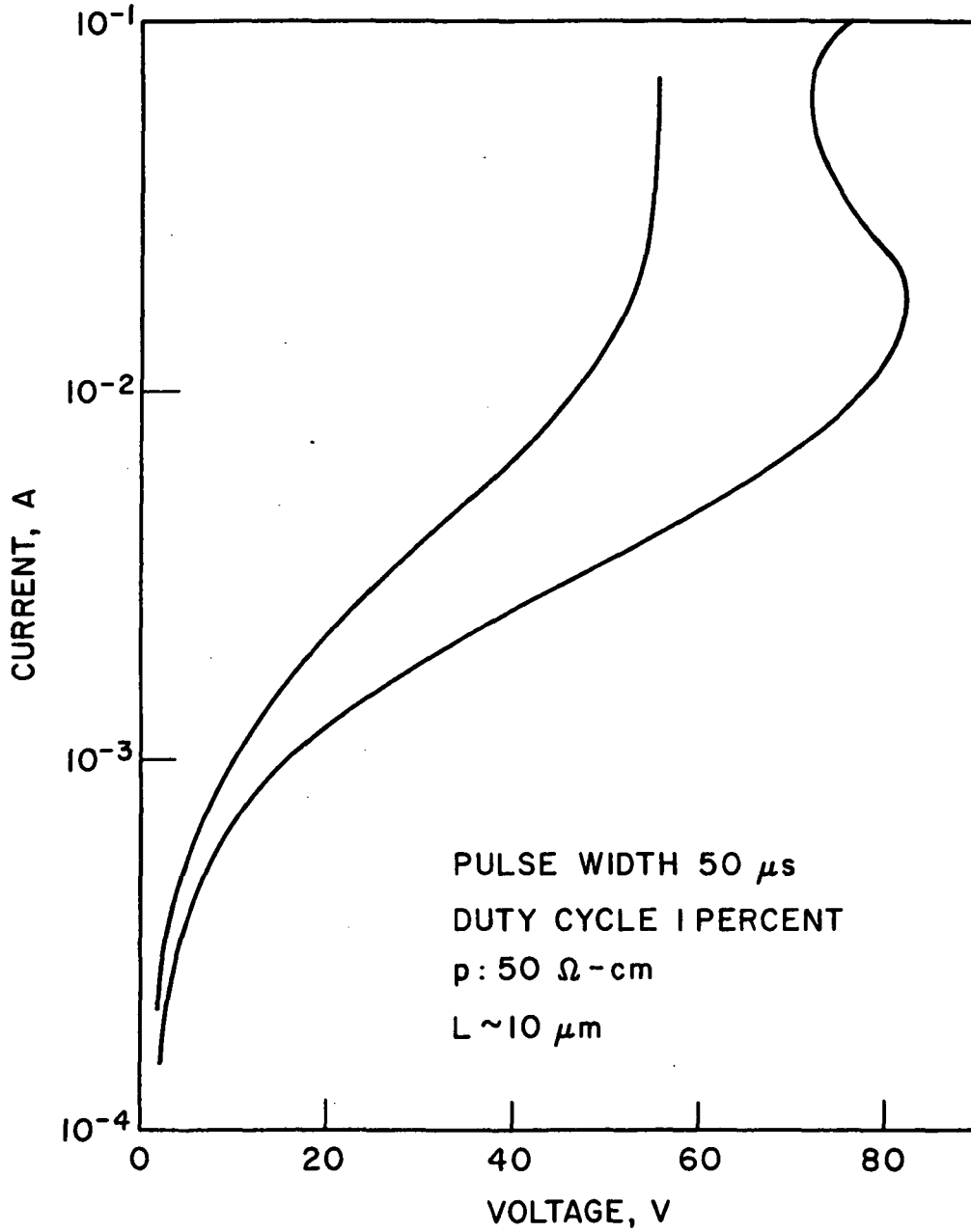


FIG. 3.4 PULSED I-V CHARACTERISTICS OF Ti-Si(p)-Ti FOR BOTH POLARITIES.

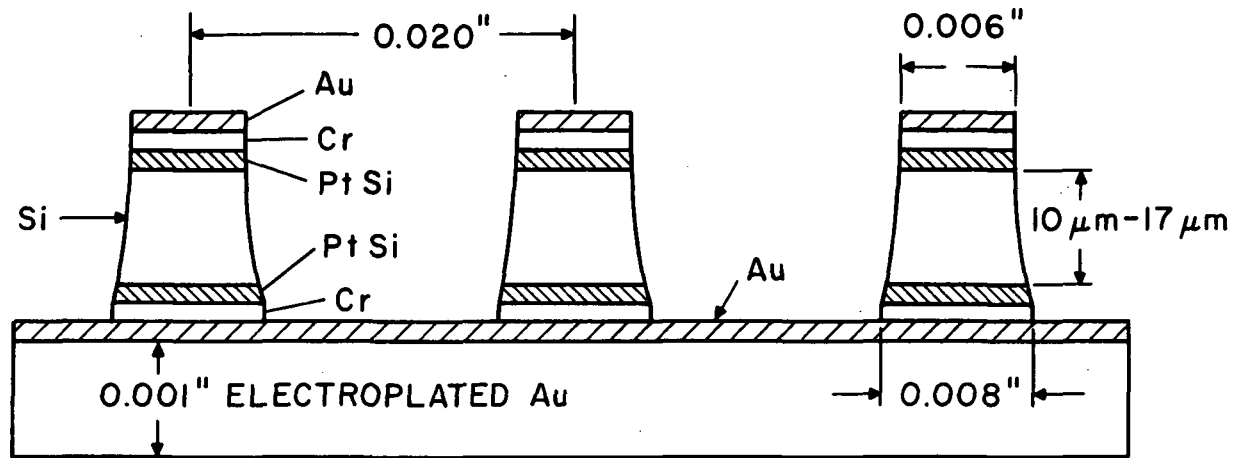
3.4 Fabrication of PtSi-Si(n)-PtSi Structures. The leaky I-V characteristics and thermal instability of Ti-Si(p)-Ti prompted the fabrication of a MINITT structure using platinum silicide barriers. An nn^+ Si wafer with an epitaxial layer having a resistivity ranging from 7 to 11 Ω -cm and a thickness of 13 to 17 μ m was mechanically thinned to less than 17 μ m. The final two steps were done using a polishing disk with 3- μ m particles followed by the standard Syton etching and polishing technique. After cleaning the wafer in acetone, Freon, HF and rinsing in DI water, the surfaces were further cleaned by backsputtering prior to sputtering a Pt layer on both sides. The sputtering is done in a dc condition in an argon plasma. The wafer is then sintered in vacuum at 650°C for ten minutes. Finally, Cr (250 Å) and Au (0.5 μ m) are evaporated on both sides. Gold is then electroplated to create a 0.001-inch thick gold base for the diodes. Circles of photoresist 0.008 inch in diameter are developed on the opposite side. The diodes are then separated by etching away sequentially the unwanted Au, Cr, PtSi, Si, PtSi and Cr. The wafer is then immersed in acetone to remove the photoresist and baked at 150°C for ten minutes at which time the diodes are ready for evaluation.

3.5 Experimental Study of I-V Characteristics of MINITT [PtSi-Si(n)-PtSi] Structures. The following MINITT devices were fabricated from an nn^+ Si wafer. The n epitaxial layer has a resistivity of 10 Ω -cm and its specified thickness ranges from 13 μ m to 17 μ m. It is etched on the substrate side using 270:28.5:5 ml HNO_3 :HF:acetic acid and 4.2 g of $NaClO_2$ solution. The finished layer does not have a uniform thickness. (Mechanical and Syton polishing is preferred, because it yields a more uniform thickness and a smoother surface.) The wafer

appears brownish on one edge and becomes increasingly more reddish toward the other edge. The measured thickness ranges from 10 μm to 17 μm . The resistivity on the reddish edge is much lower than that on the other edge indicating that a very thin layer of substrate or its interface with the epitaxial layer still exists on the thicker side. MINITT's are then fabricated according to the procedure mentioned earlier. The etching process needed for diode separation results in an undercutting of Si just underneath the metal layers. These unwanted rims of the metal layers are removed by ultrasonic cleaning. The final resultant structures are shown in Fig. 3.5.

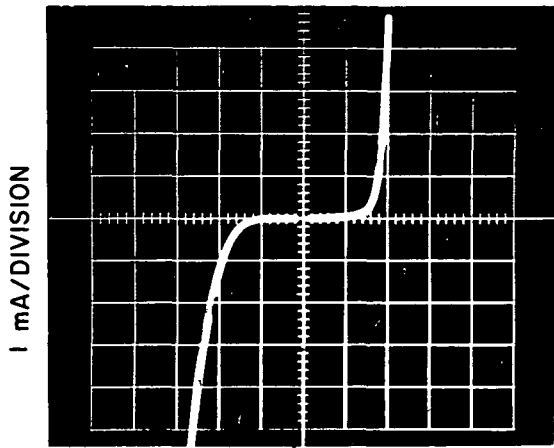
The I-V characteristics of MINITT's, with increasing thickness are shown in Figs. 3.6a-c. Figure 3.6d corresponds to one end with a thin layer of substrate or its interface, which is characterized by very low resistivity. It is actually a Schottky-barrier diode with a "bad" ohmic contact. The breakdown voltage of approximately 40 V or higher corresponds to the theoretical value $V_{RT} \geq 38.4$ V for epitaxial layer thickness $\geq 10 \mu\text{m}$. The increase of breakdown voltage with the thickness and the exponential rise of current for voltage exceeding the reach-through voltage are the observed characteristics also reported elsewhere.¹

The asymmetry in the I-V characteristics is due to the difference in the nature of the barriers. The I-V characteristics to the left correspond to the etched junction side being reverse biased and those to the right, the same junction forward biased. It is suggested that the etched junction when forward biased is less efficient in emitting holes than the other one. Therefore, a considerably higher voltage has to be applied across the diode before achieving enough hole injections on the forward-biased junction to cause rapid current rise. Hence, the right-hand side I-V characteristics



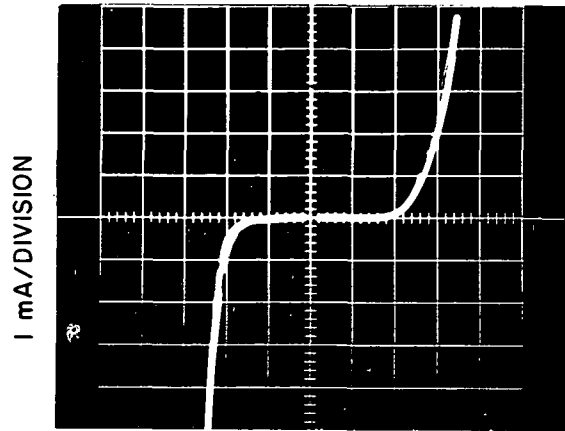
Au 0.5 μm THICK
Cr 250 \AA THICK
Pt Si 300 \AA THICK

FIG. 3.5 PHYSICAL STRUCTURES OF MINITT DEVICES ON A COMMON GOLD BASE.



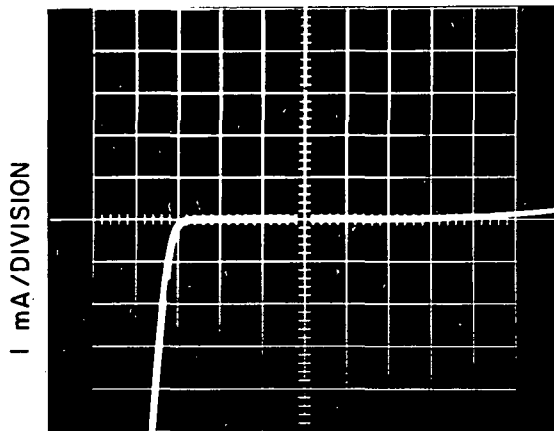
20 V/DIVISION

(a)



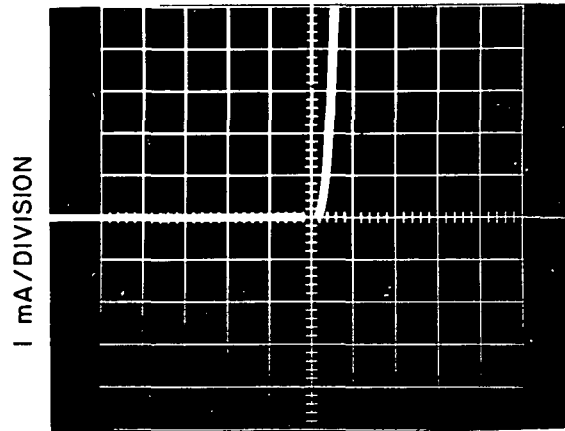
20 V/DIVISION

(b)



20 V/DIVISION

(c)



20 V/DIVISION 5 V/DIVISION

(d)

FIG. 3.6 I-V CHARACTERISTICS OF MINITT DEVICES.

has a higher reach-through voltage than that of the left-hand side. This behavior is further supported by Fig. 3.6d in which the right-hand side junction is effectively an ohmic contact which can emit few holes when it is forward biased. Thus with the etched side reverse biased, no reach-through characteristics are observed in the I-V trace because no minority holes are injected. It is suggested that the curvature introduced by undercutting of Si during etching distorted the field at that junction causing the barrier to be lowered. This barrier lowering could lead to a less efficient injection of holes.

3.6 Theoretical dc I-V Characteristic of the MINITT Structure.

Considerable simplifications can be made in the calculations if the I-V characteristic is separated into prepunch-through and postpunch-through regions. For voltages below

$$V_{RT} \cong \frac{q}{\epsilon} \frac{N_o L^2}{2}$$

the current is quite small and is given by the reverse saturation current of one barrier as

$$J = A^{**} T^2 \exp\left(-\frac{q(\phi_{Bn} - \Delta\phi)}{kT}\right) \left(\exp \frac{qV}{kT} - 1\right), \quad (3.3)$$

where V is the applied voltage and the definitions of the other terms can be found in Section 6 of this report.

For postpunch through it is assumed that the band minimum reaches the metal contact which is forward biased causing the boundary condition $E(0) = 0$ for the electric field. The pertinent equations become

$$\frac{\partial J}{\partial x} = 0, \quad (3.4)$$

$$J = qp v \quad (3.5)$$

and

$$\epsilon \frac{\partial E}{\partial x} = q(N_D + p), \quad (3.6)$$

where the velocity is not quite saturated and is assumed to vary as

$$v = \mu E_0^{1/2} E^{1/2}, \quad (3.7)$$

where μ is the low-field mobility, E_0 is some critical field obtained from measurement of mobility and diffusion has been neglected. The I-V characteristic is then given by parametric equations of current and voltage as²

$$V = \left(\frac{L^2 \mu^2 N_D}{6\epsilon} \right) \frac{3 e^{2u} - 16(3/2)u + 36 e^u - 48 e^{u/2} + 6u + 25}{(e^u - 4 e^{u/2} + u + 3)^2},$$

$$J = \left(\frac{L \mu^2 N_D E_0}{\epsilon} \right)^{1/2} (e^u - 4 e^{u/2} + u + 3)^{-1/2}, \quad (3.8)$$

where

$$u \equiv \frac{N_D s}{\epsilon} \quad \text{and} \quad s \equiv \int_0^x \frac{dx}{E}.$$

2. Dacey, C. D., "Space-Charge-Limited Hole Current in Ge," Phys. Rev., vol. 90, No. 5, pp. 759-763, June 1953.

The current given in Eq. 3.8 was found to behave roughly as an exponential of voltage. In summary, the current behaves as a saturation current at prepunch through and varies roughly exponentially, as seen experimentally and as reported by Coleman and Sze,¹ in the punch-through region.

A refinement of the current expression at prepunch through is possible. Consider the case of a leaky structure in which the space charge induced due to current is significant. In the extreme case of low doping level, the equations are

$$\epsilon \frac{dE}{dx} = \rho \quad (3.9)$$

and

$$J = D \frac{d\rho}{dx} - \mu\rho E, \quad (3.10)$$

where diffusion has been included and low-field mobility is assumed. The I-V characteristic is given by

$$J = \frac{9}{8} \frac{\epsilon\mu}{L^3} V^2. \quad (3.11)$$

In reality the current at prepunch through should resemble somewhat the saturation current and Child's law.

3.7 Program for the Next Period. Fabrication of platinum silicide MINITT structures will be continued and the I-V characteristics will be compared with the theory. The microwave performance of such diodes will be measured and compared with the results of a large-signal analysis.

4. Intermodulation Products in IMPATT Diode Amplifiers

Supervisors: G. I. Haddad and N. A. Masnari

Staff: R. J. Trew

4.1 Introduction. The objective of this phase of the program is to determine the intermodulation characteristics of an IMPATT diode operated in a reflection amplifier circuit under multifrequency conditions. During this period a circuit for two-frequency operation of an IMPATT diode reflection amplifier was constructed. This circuit was used to obtain data for operation of the amplifier with two, equal amplitude, input signals.

4.2 Test Setup. The experimental amplifier consisted of a silicon IMPATT diode positioned in a 50- Ω coaxial cavity. The amplifier was tuned by adjusting two movable tuning slugs; one having a length of one-quarter wavelength at 8 GHz and the other a length of one-quarter wavelength at 10 GHz. The impedance of each slug was 20 Ω . The amplifier circuit is shown in Fig. 4.1. The circuit has provision for two-frequency operation by introducing the signals to the amplifier through a magic tee. The magic tee allows the input signals to be controlled independently although there is a power loss of 3 dB at the input due to the power absorbed in the termination arm. The power measurements at the individual frequencies were made using the spectrum analyzer which was calibrated so that the relative power levels could be obtained directly from the display.

4.3 Single-Frequency Operation. Operation of the amplifier at high bias currents (e.g., above 50 mA) and high RF power input levels (e.g., above 10 mW) caused considerable difficulty due to oscillations induced in the circuit at C-band. It has been shown¹ that oscillation at

1. Schroeder, W. E. and Haddad, G. I., "Effect of Harmonic and Subharmonic Signals on Avalanche-Diode Oscillator Performance," IEEE Trans. on Microwave Theory and Techniques, vol. MTT-18, No. 6, pp. 327-331, June 1970.

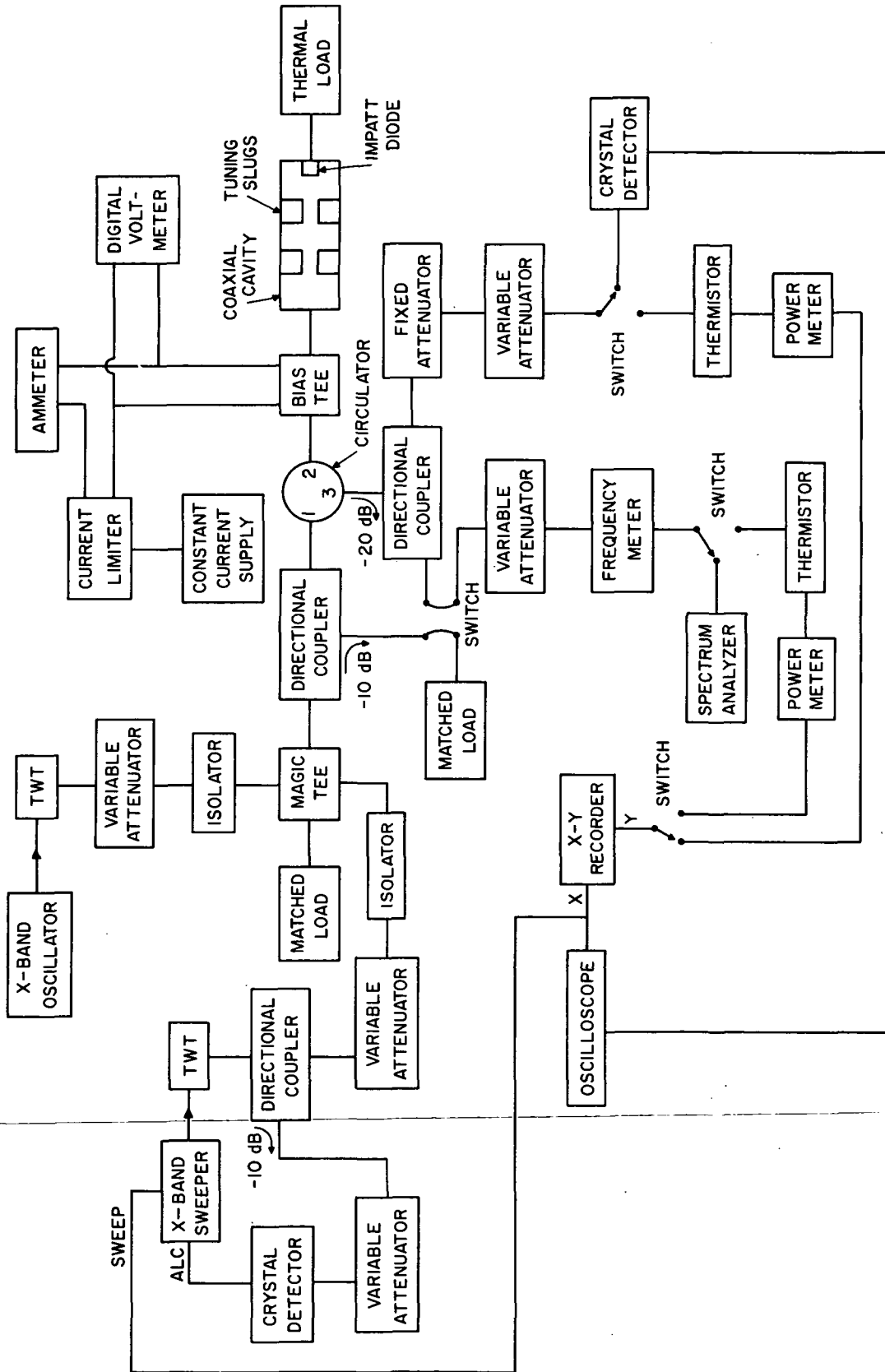


FIG. 4.1 TWO-FREQUENCY TEST APPARATUS FOR AN IMPATT DIODE REFLECTION AMPLIFIER.

X-band can induce negative conductance at lower frequencies. Apparently the output circuit admittance is such that a negative match exists with the diode when it is operated under high-power conditions thus allowing the lower-frequency oscillations to occur. These oscillations or instabilities can be significantly reduced by positioning the tuning slugs close to the diode. With the slugs positioned in this manner it was possible to operate the diode at 70 mA of bias current and 100 mW of input power with no C-band oscillations.

With the diode biased at 40 mA of dc current it was possible to obtain 30 dB of small-signal gain with little difficulty. There was very little difference in tuning ease or maximum gain obtainable with the slugs either near the diode or at the extreme end of the coaxial cavity. However, positioning the slugs near the diode allowed for more sensitive tuning and reduced the C-band oscillation problem. For the intermodulation tests the diode bias current was held at 40 mA and the amplifier was tuned to provide 22 dB of small-signal gain at a frequency of 9.445 GHz. The single-frequency gain curves are shown in Fig. 4.2. As the RF input power is increased from 0.01 mW to 10 mW the maximum gain is reduced to 8.8 dB, the frequency of maximum gain is shifted from 9.445 GHz to 9.385 GHz and the 3-dB bandwidth is increased from 24 MHz to 190 MHz.

4.4 Two-Frequency Operation. For the first set of intermodulation tests the higher frequency (F_2) was held constant at 9.445 GHz while the second signal (F_1) was placed 3 MHz lower in frequency at 9.442 GHz. Three additional runs were made with the frequency separation increased to 10 MHz, 30 MHz and 100 MHz, respectively, while holding F_2 constant at 9.445 GHz. Power input vs. power output data was taken for both F_1 and F_2 under single-frequency conditions. The experiment was repeated with

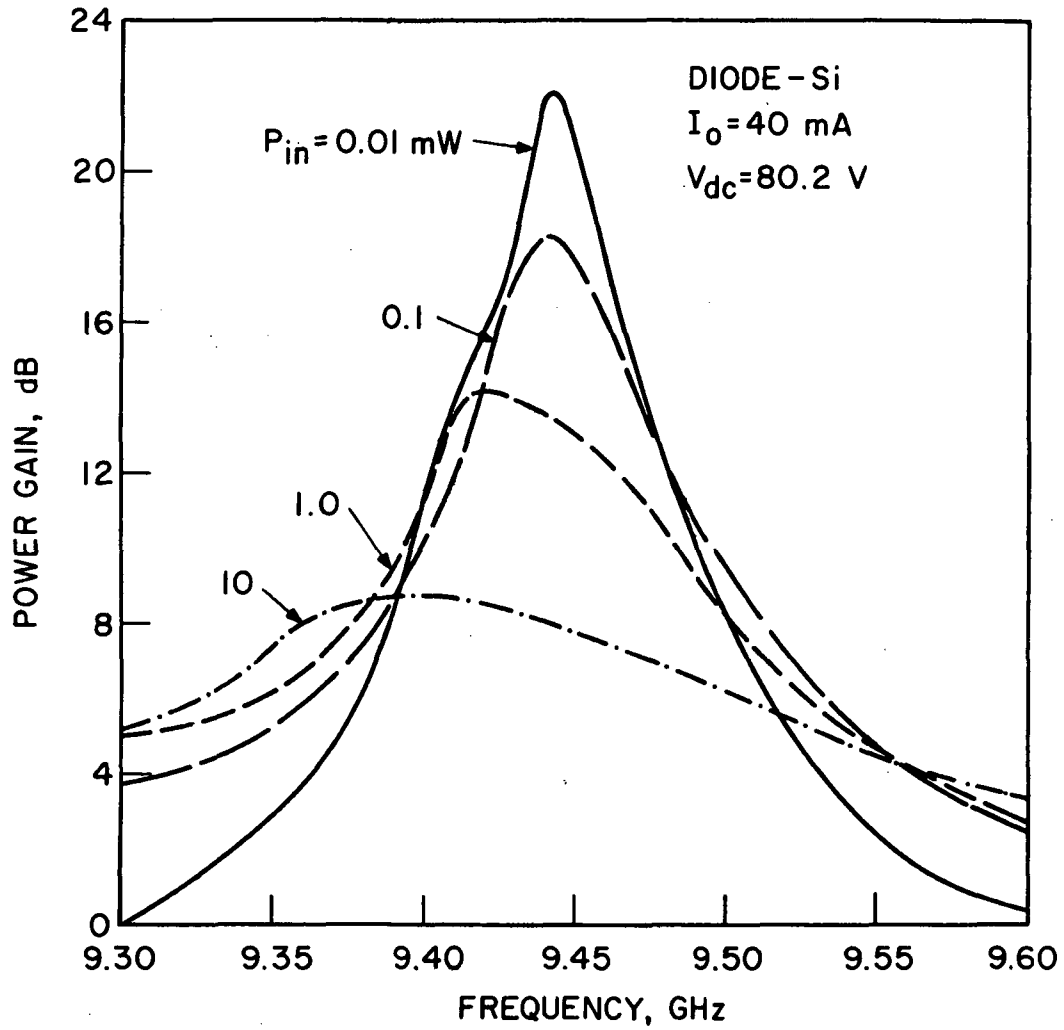


FIG. 4.2 SINGLE-FREQUENCY GAIN CHARACTERISTIC FOR AN IMPATT DIODE REFLECTION AMPLIFIER.

equal input signals F_1 and F_2 and the output powers for F_1 and F_2 and the most significant intermodulation products were recorded. The intermodulation products are given by the well-known sum and difference frequency mixing laws of nonlinear device operation and can be expressed as

$$F_i = nF_1 \pm mF_2 ,$$

where n and m are positive integers. In the test results the intermodulation products are identified as $F_3 = 2F_1 - F_2$, $F_4 = 2F_2 - F_1$ and $F_5 = 3F_1 - 2F_2$. The second set of tests were identical with the first except that F_1 was fixed at the point of maximum small-signal gain (i.e., 9.445 GHz) and F_2 was set at frequencies higher than F_1 for the same frequency separations as those given previously.

The power curves for F_2 fixed at 9.445 GHz and a frequency separation of 3 MHz are given in Fig. 4.3. Since the point of maximum gain shifts from 9.445 GHz to a lower frequency by 60 MHz for input power levels from -20 dBm to 10 dBm, it is expected that the intermodulation products at the lower frequencies will be increased as the maximum gain shifts through them.

Figure 4.3 ($\Delta f = 3$ MHz) indicates that the two single-frequency power curves are approximately the same. At such small frequency separations the two signals see essentially the same gain and hence the curves are similar. The data also indicates that the curves cease to be linear at low input power levels (i.e., -16 dBm). This behavior was typical for all cases in which the signal was tuned for large small-signal gain. When the test was repeated for both input signals present it was found that the F_1 and F_2 signals, although still experiencing about the same gain, were not generating as much output power as for the single-frequency case. The power

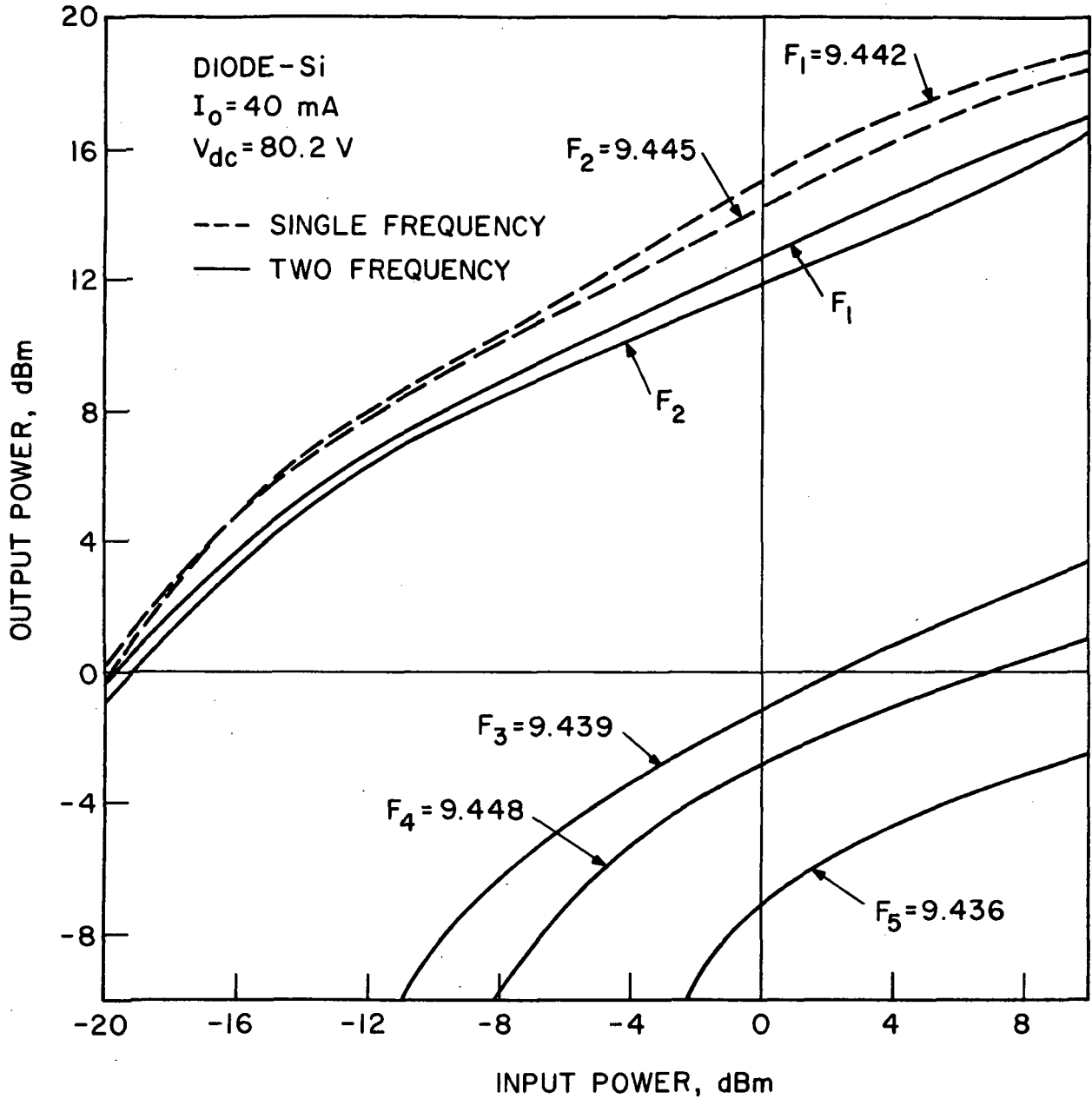


FIG. 4.3 DYNAMIC CHARACTERISTICS OF AN IMPATT DIODE REFLECTION AMPLIFIER FOR TWO EQUAL AMPLITUDE INPUT SIGNALS. ($\Delta f = 3 \text{ MHz}$)

lost by F_1 and F_2 appears in the form of intermodulation products F_3 , F_4 , F_5 , etc. The intermodulation products increase in magnitude with increasing input power with $|F_3| > |F_4| > |F_5|$. With 10 dBm of input power the largest intermodulation product F_3 is approximately 13 dB down from the amplified input signals. Figure 4.4 was plotted from data obtained by increasing the frequency separation to 10 MHz by placing F_1 at 9.435 GHz. As in the $\Delta f = 3$ MHz test the single-frequency curves for F_1 and F_2 are approximately the same. However, it can be seen that F_2 is initially at a higher output level since it is located at the point of maximum small-signal gain but shifts to an output level lower than F_1 as the input power is increased. This is due to the shift in the point of maximum gain through F_1 with increasing power level. The two-frequency curves are lower in output power level than the single-frequency curves and also show the power level crossover effect, although at a lower input power level than the single-frequency cases. The intermodulation products F_3 , F_4 and F_5 indicate that $|F_3| > |F_4| > |F_5|$ at lower input power levels. As the input power is increased to approximately 5 dBm F_5 becomes larger in magnitude than F_4 . Again, this is due to the shift in the gain characteristics so that the lower-frequency components are amplified more than the higher-frequency components. With 10 dBm of input power in each signal the largest intermodulation product, F_3 is approximately 11 dB down from the amplified input signals F_1 and F_2 .

When the frequency separation is increased to 30 MHz by placing F_1 at 9.415 GHz (Fig. 4.5) it is seen that the single-frequency and two-frequency curves for F_1 and F_2 are initially the same. At low input power levels there is no change in the output power of one signal due to the presence of the second signal. Since F_1 is initially at a low gain position

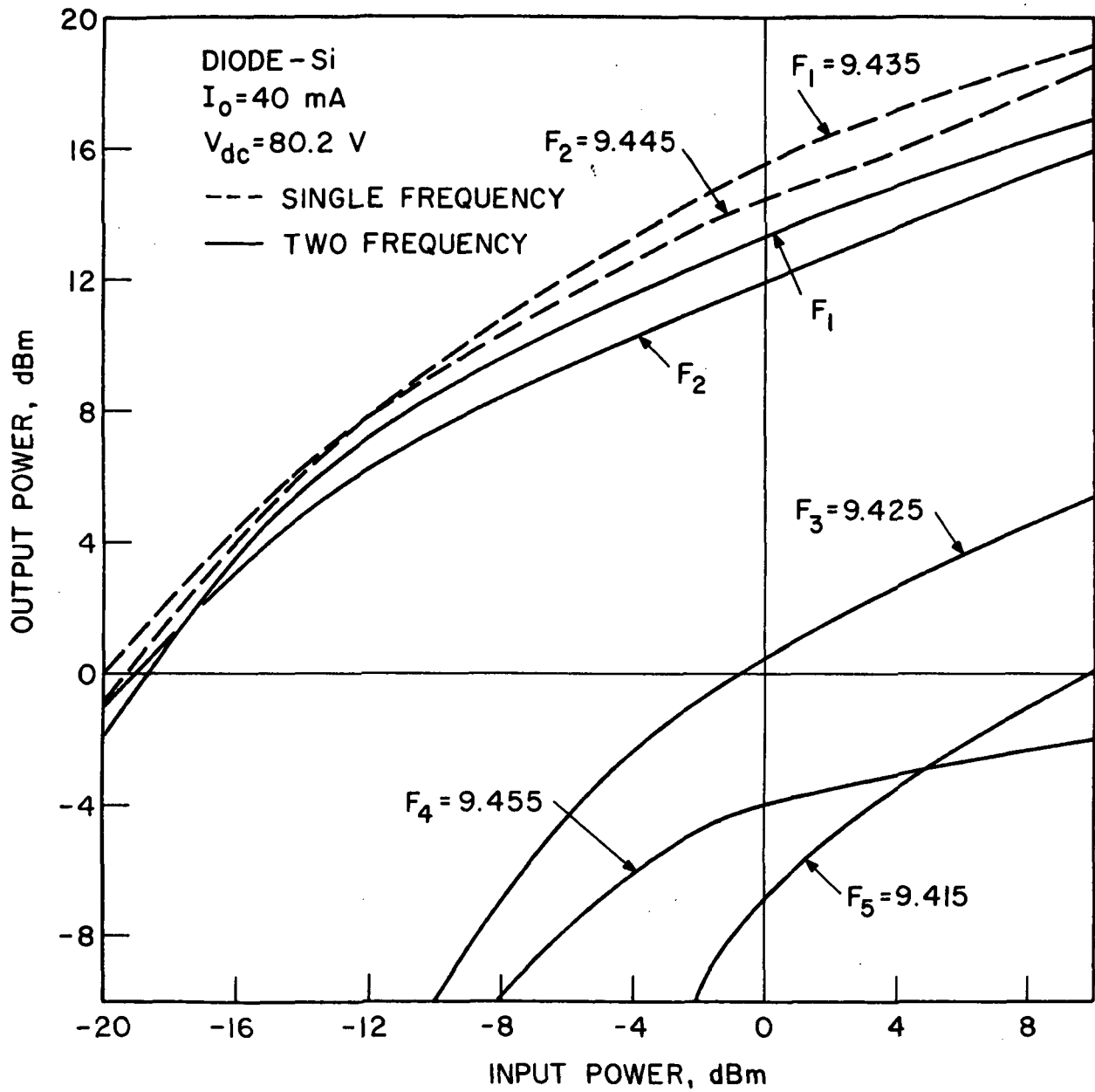


FIG. 4.4 DYNAMIC CHARACTERISTICS OF AN IMPATT DIODE REFLECTION AMPLIFIER

FOR TWO EQUAL AMPLITUDE INPUT SIGNALS. ($\Delta f = 10 \text{ MHz}$)

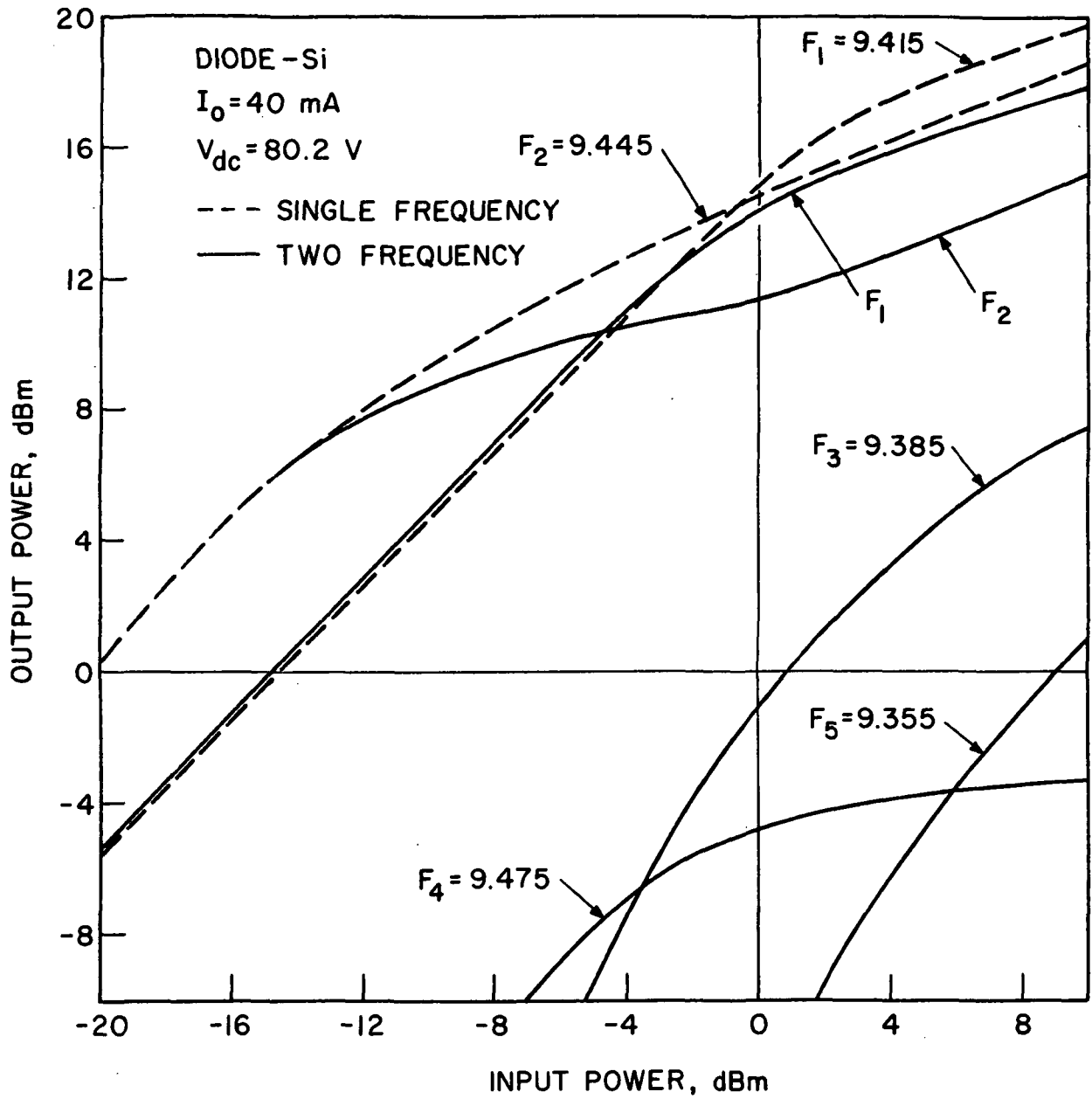


FIG. 4.5 DYNAMIC CHARACTERISTICS OF AN IMPATT DIODE REFLECTION AMPLIFIER FOR TWO EQUAL AMPLITUDE INPUT SIGNALS. ($\Delta f = 30 \text{ MHz}$)

(Fig. 4.2) its curve does not show saturation effects until much later than the curve for F_2 . Both the single-frequency and two-frequency curves for F_1 and F_2 show the output power crossover effect. The intermodulation effects start to become evident at -11 dBm of input power where the single-frequency and two-frequency curves for F_2 start to separate with the two-frequency curve losing output power compared to the single-frequency curve. The high-frequency intermodulation product F_4 is the first to appear. This is because the higher-frequency output signal F_2 initially is much larger in magnitude than F_1 due to the position of the two frequencies on the gain curve (Fig. 4.2). This causes the mixing mechanism to put more energy into the higher-frequency intermodulation product until the gain shift forces the magnitude of F_1 to equal and then exceed the magnitude of F_2 . As this occurs, the lower-frequency products F_3 and finally F_5 become larger than F_4 . With 10 dBm of input power, F_3 is down only about 8 dB from the amplified input signal F_2 .

Increasing the separation to 100 MHz (Fig. 4.6) results in little interaction between the two signals. The single-frequency and two-frequency curves for both F_1 and F_2 are essentially the same. F_1 initially is at a low output power level because it is off the large gain peak at low input power levels. It increases in output power level as the gain peak shifts toward it and remains linear throughout the power range investigated. The high-frequency intermodulation product F_4 is the largest for the same reason as in the 30 MHz separation case. With 10 dBm input power, F_4 is approximately 19 dB down from the amplified input signals.

For the second set of tests, the signal F_1 was set at 9.445 GHz (i.e., point of maximum small-signal gain) and the signal F_2 was placed at higher frequencies for separations of 3 MHz, 10 MHz, 30 MHz and 100 MHz.

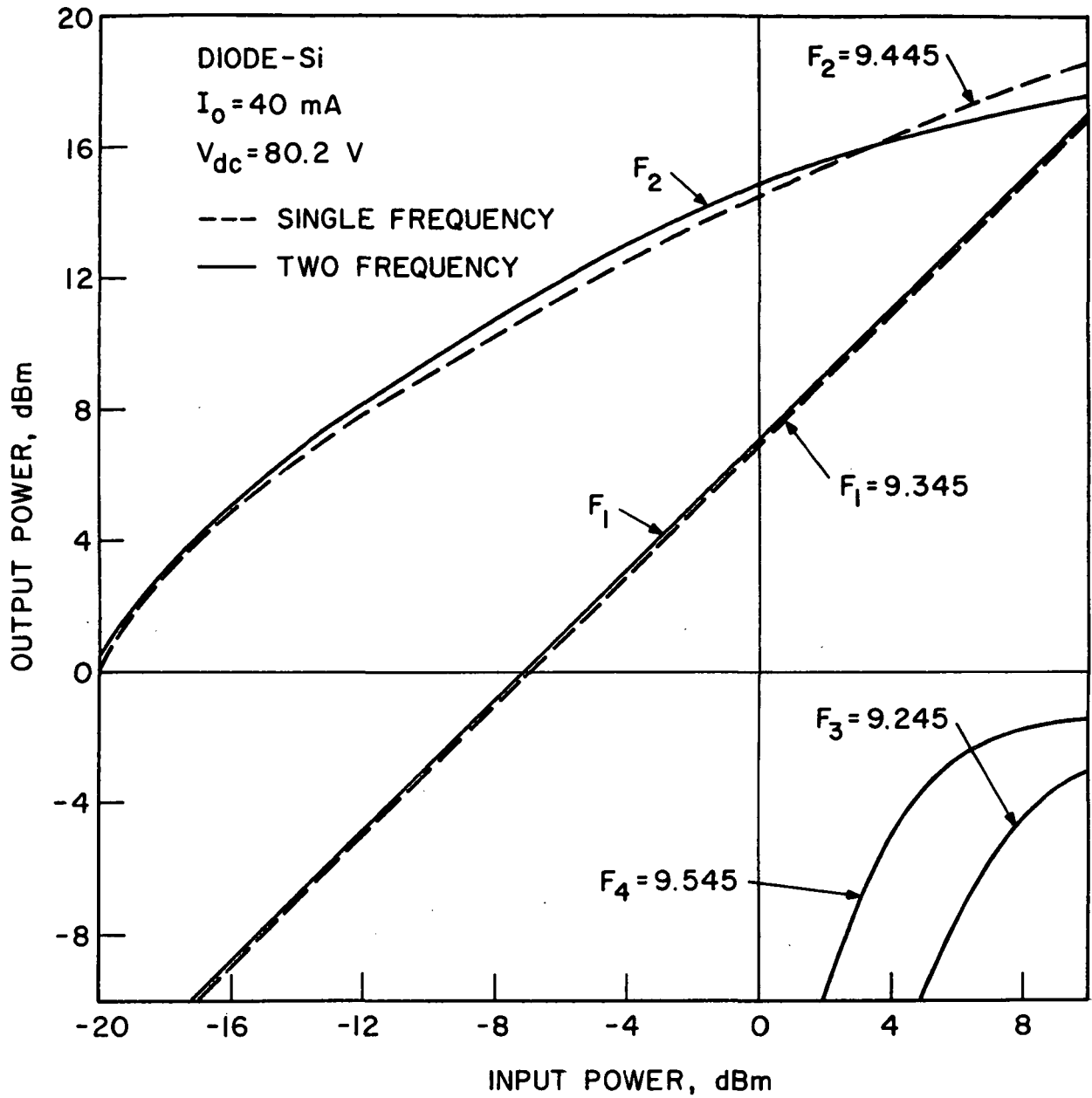


FIG. 4.6 DYNAMIC CHARACTERISTICS OF AN IMPATT DIODE REFLECTION AMPLIFIER FOR TWO EQUAL AMPLITUDE INPUT SIGNALS. ($\Delta f = 100 \text{ MHz}$)

The 3 MHz separation test had essentially the same behavior as that illustrated in Fig. 4.3. The 10 MHz separation test (Fig. 4.7) resulted in no output power crossover effect as F_1 is always larger than F_2 . Both low-frequency intermodulation products F_3 and F_5 are larger than the high-frequency product F_4 . These results are due to the gain peak shift and the consequent amplification increase at lower frequencies. The largest intermodulation product F_3 is 11 dB down from the original signals with 10 dBm of input power.

The 30 MHz (Fig. 4.8) and 100 MHz tests produced essentially the same results. The single-frequency and two-frequency curves are approximately the same for both F_1 and F_2 . The figures again show low-frequency dominance as F_3 and F_5 , the low-frequency intermodulation products, are always greater than the high-frequency intermodulation signal F_4 .

4.5 Conclusions. Small-signal, single-frequency gains in the neighborhood of 30 dB are easily obtained in a double slug tuned coaxial IMPATT diode reflection amplifier. With increasing RF input power the single-frequency gain decreases, the point of maximum gain shifts to a lower frequency and the bandwidth increases.

Operating the amplifier with two equal amplitude input signals results in the generation of sum and difference frequency intermodulation products. The shift in the maximum gain with increasing RF input power provides a low-frequency dominance mechanism affecting both the amplified source signals and the intermodulation products. ~~It is possible for the~~
low-frequency second-order intermodulation products to be greater in magnitude than the high-frequency first-order intermodulation products, depending on where the original signals are located relative to the

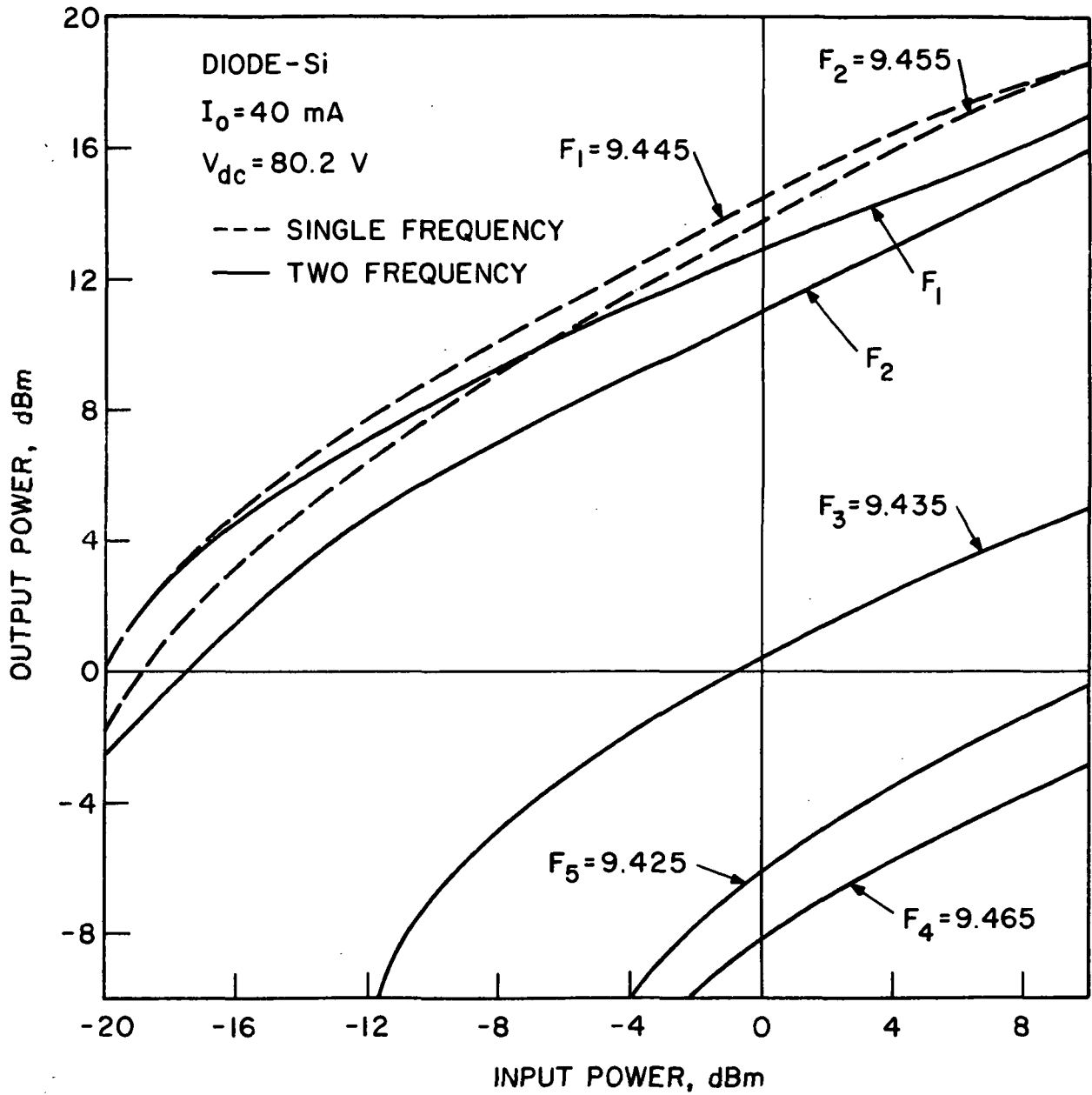


FIG. 4.7 DYNAMIC CHARACTERISTICS OF AN IMPATT DIODE REFLECTION AMPLIFIER FOR TWO EQUAL AMPLITUDE INPUT SIGNALS. ($\Delta f = 10 \text{ MHz}$)

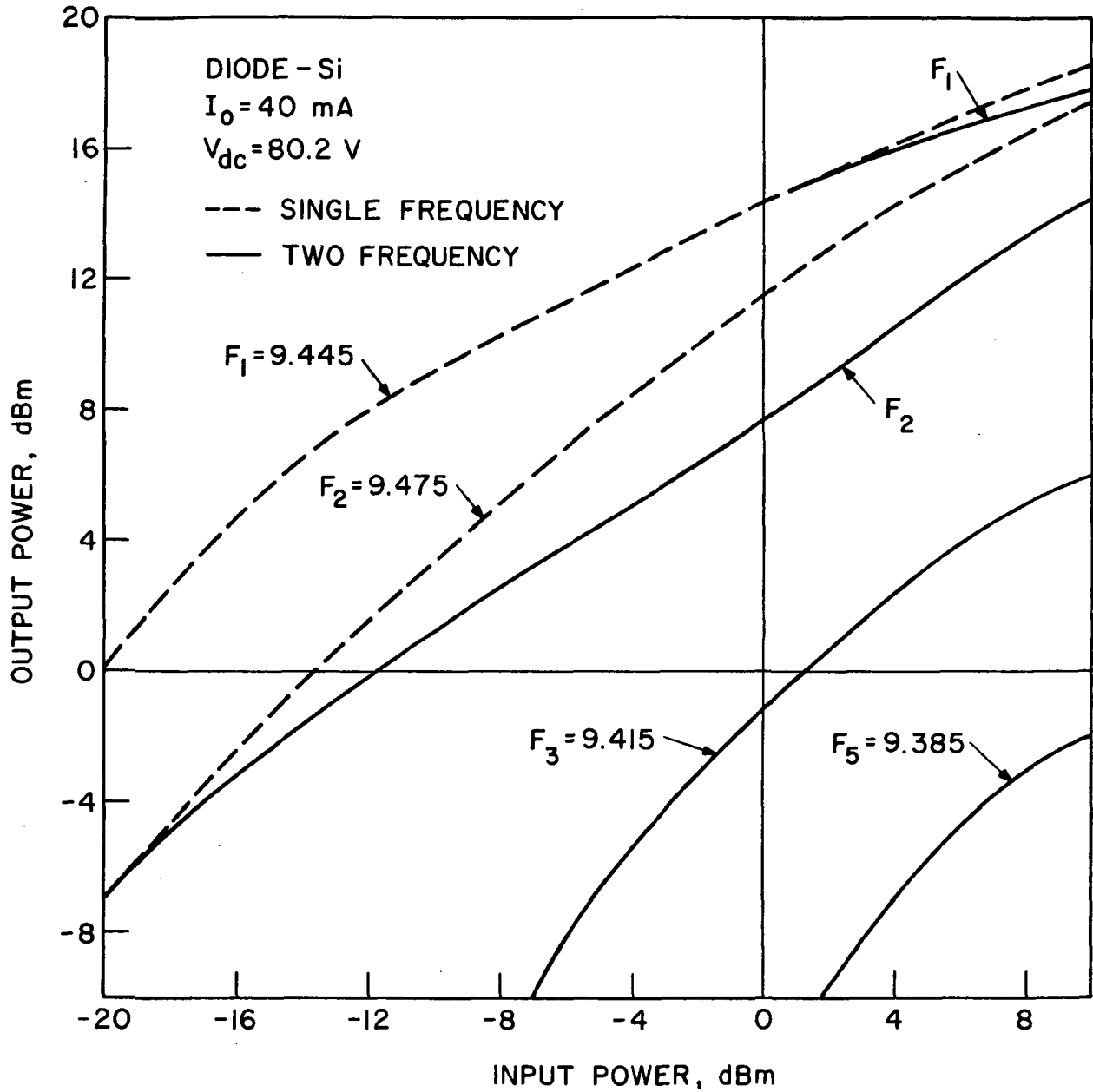


FIG. 4.8 DYNAMIC CHARACTERISTICS OF AN IMPATT DIODE REFLECTION AMPLIFIER FOR TWO EQUAL AMPLITUDE INPUT SIGNALS. ($\Delta f = 30 \text{ MHz}$)

amplifier gain characteristics. As the frequency separation between the two original signals is increased the interaction between the signals (in terms of the output power generated at the source frequencies and intermodulation products) is decreased.

4.6 Program for the Next Period. Intermodulation tests will be conducted for several different frequencies in X-band. The tests will be extended to input power levels large enough to reduce the maximum gain to approximately 3 dB in order to investigate the limiting behavior of the amplifier. These tests will also be conducted on GaAs diodes as soon as appropriate devices are obtained.

5. Harmonic Generation Using Read Diode Varactors

Supervisor: G. I. Haddad

Staff: K. K. Dutta Choudhury

5.1 Introduction. The mathematical formulation of the C-V characteristic of the Read diode and its possible application as a harmonic generator were presented in the previous report. The theoretical small- and large-signal second-harmonic conversion efficiency and normalized power output of a certain assumed realizable model of a Read diode varactor are presented here. For comparison, the small- and large-signal second-harmonic conversion efficiency and normalized power output of certain kinds of commercially available punch-through varactors are also evaluated. The agreement between the large-signal varactor analysis and the results obtained by Grayzel¹ is excellent.

1. Grayzel, A. I., "Design Parameters for Overdriven Varactor Frequency Doublers Using Punch-Through or Bimode Varactors," IEEE Trans. on Microwave Theory and Techniques (Correspondence), vol. 17, No. 6, pp. 345-347, June 1969.

It is worth mentioning that the mathematical formulation of the Read diode varactor problem can be utilized for studying varactors having different types of C-V characteristics by modifying certain parameter values.

5.2 Power Output and Efficiency of a Read Diode Varactor. In order to study both the large- and small-signal characteristics of Read diode varactors as second-harmonic generators, Eq. 6.24 of Semiannual Progress Report No. 91 has been changed in the following manner for greater adaptability:

$$\bar{Q}_1 \leq \frac{\bar{Q}_{\max} - \bar{Q}_{\min}}{\left[3 + \left(1 + 32 \frac{\bar{Q}_2^2}{\bar{Q}_1^2} \right)^{1/2} \right] \left\{ \frac{1}{2} + \frac{\bar{Q}_1^2}{32\bar{Q}_2^2} \left[\left(1 + 32 \frac{\bar{Q}_2^2}{\bar{Q}_1^2} \right)^{1/2} - 1 \right] \right\}^{1/2}} \quad (5.1)$$

This change in the form of the equation makes it easier to study both the large- and small-signal characteristics of a diode by choosing the appropriate range of $(\bar{Q}_{\max} - \bar{Q}_{\min})$, where \bar{Q} refers to the normalized charge stored in the diode.

For a large-signal analysis the diode is overdriven so that

$$\bar{Q}_{\max} = 1 \quad (5.2)$$

and

$$\bar{Q}_{\min} = -1 \quad (5.3)$$

For a small-signal analysis, \bar{Q}_{\max} and \bar{Q}_{\min} have been defined in the following manner:

$$\bar{Q}_{\max} = \bar{q}'_{pt} + 0.01 \times N_2 (1 - \bar{q}'_{pt}) \quad (5.4)$$

and

$$\bar{Q}_{\min} = 0.01 \times N_1 \times \bar{q}'_{pt} \quad (5.5)$$

where \bar{q}_{pt} and \bar{q}'_{pt} refer to the normalized charges at the normalized breaking voltages \bar{v}_{pt} and \bar{v}'_{pt} of the C-V characteristic. N_2 and N_1 values fix the region of the C-V characteristic where the diode is allowed to operate.

In particular, $N_1 = 0$ and $N_2 = 100$ correspond to a fully driven diode.

The models shown in Figs. 5.1 and 5.2 have been taken for studying the conversion characteristics of a Read diode and a punch-through varactor, respectively. The pertinent results of the large-signal analysis of these two models are tabulated in Table 5.1, where \bar{v}_{pt} = the normalized punch-through voltage, \bar{v}'_{pt} = the normalized voltage beyond which capacitance remains constant at C_{min} , $\gamma_{1,2}$ = the exponents of capacitance variation in Regions I and II, respectively, as indicated in Figs. 5.1 and 5.2 and $\omega_c = 1/C_{min}R_s$ is the cutoff frequency of the diode.

Table 5.1

Tabulation of Large-Signal Normalized Power Output and Efficiency of Read Diode and Punch-Through Varactors

$$(\gamma_1 = 0.5, \bar{v}_{pt} = 0.2, \omega_{out}/\omega_c = 10^{-2})$$

γ_2	\bar{v}'_{pt}	Normalized Power Output (β)	Efficiency E_{ff}
4.0	0.3	0.13750	84.718
0	0.2	0.07293*	94.653*
0.1	1.0	0.07880*	94.069*
0.2	1.0	0.08520*	93.393*

* The results agree with those of Grayzel.¹

The small-signal efficiency and normalized power output of the Read diode model of Fig. 5.1 are presented in Figs. 5.3 and 5.4, respectively. The same quantities for the diode of Fig. 5.2 are presented in Figs. 5.5 and 5.6, respectively.

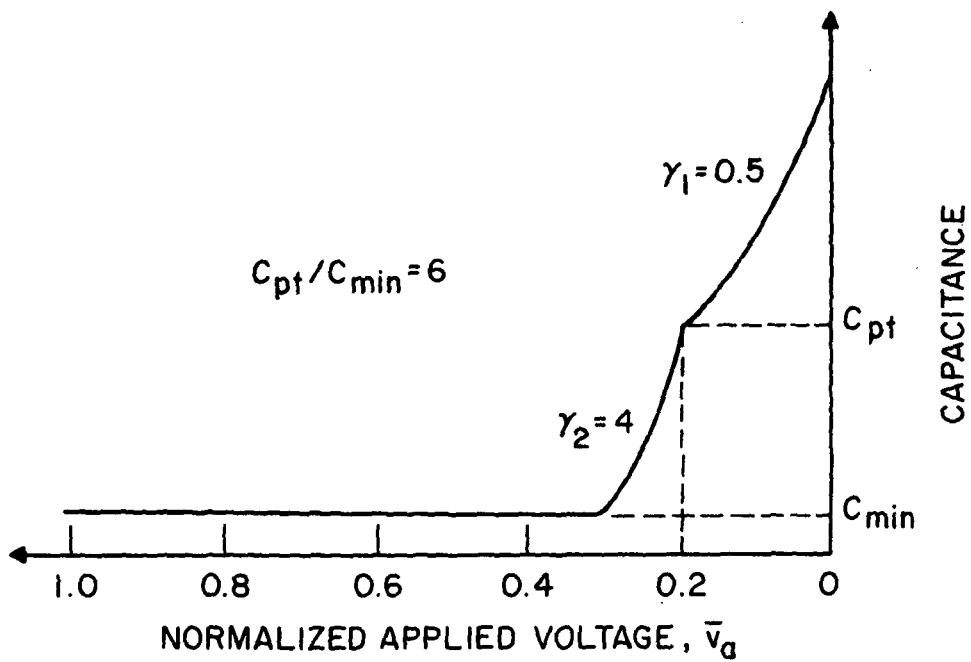


FIG. 5.1 C-V CHARACTERISTIC OF A READ DIODE VARACTOR.

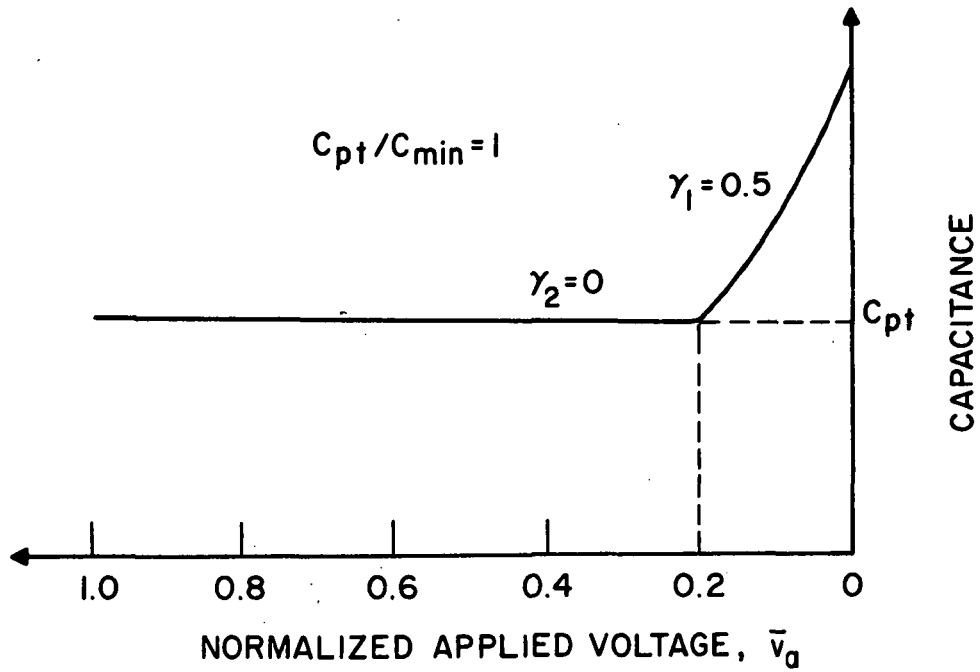


FIG. 5.2 C-V CHARACTERISTIC OF AN IDEAL PUNCH-THROUGH VARACTOR.

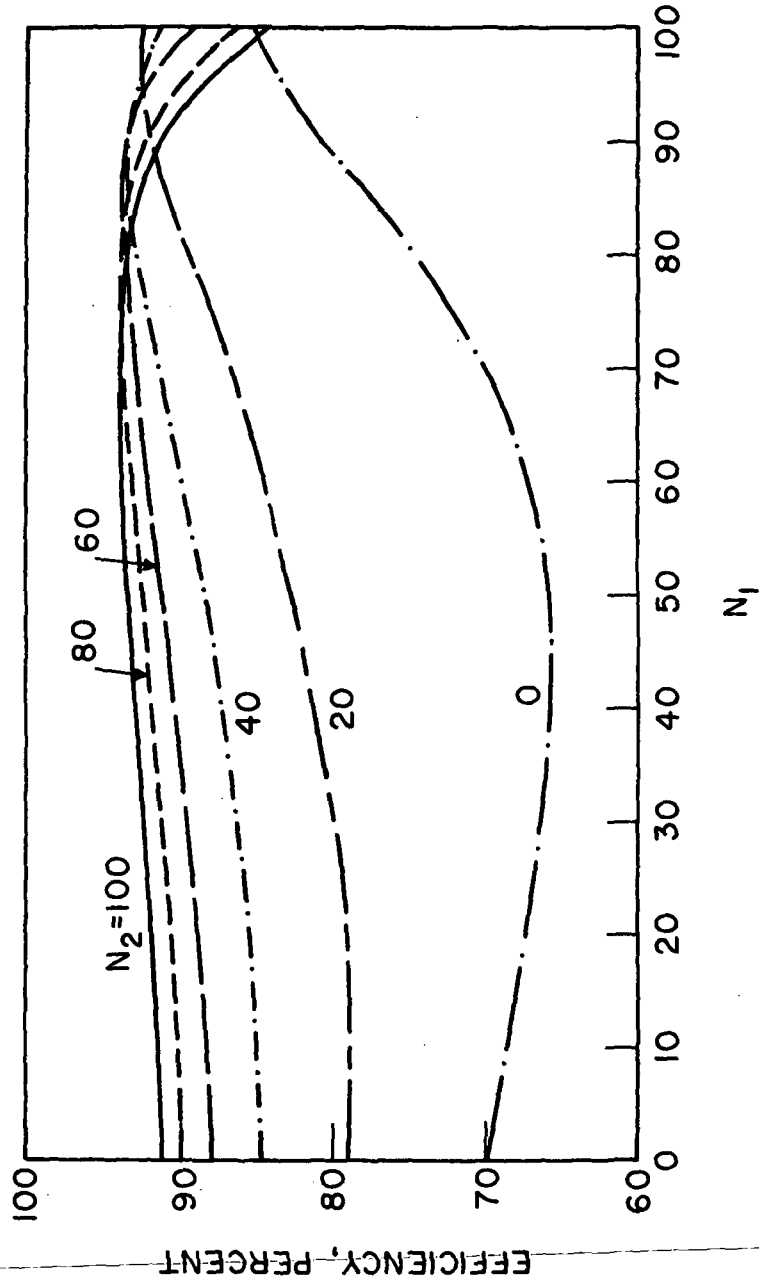


FIG. 5.3 THEORETICAL EFFICIENCY OF THE READ DIODE VARACTOR OF FIG. 5.1 FOR DIFFERENT N_1 AND N_2 VALUES. ($\gamma_1 = 0.5$, $\gamma_2 = 4$, $\bar{v}_{pt} = 0.2$, $\bar{v}'_{pt} = 0.3$, $\omega_{out}/\omega_c = 10^{-2}$)

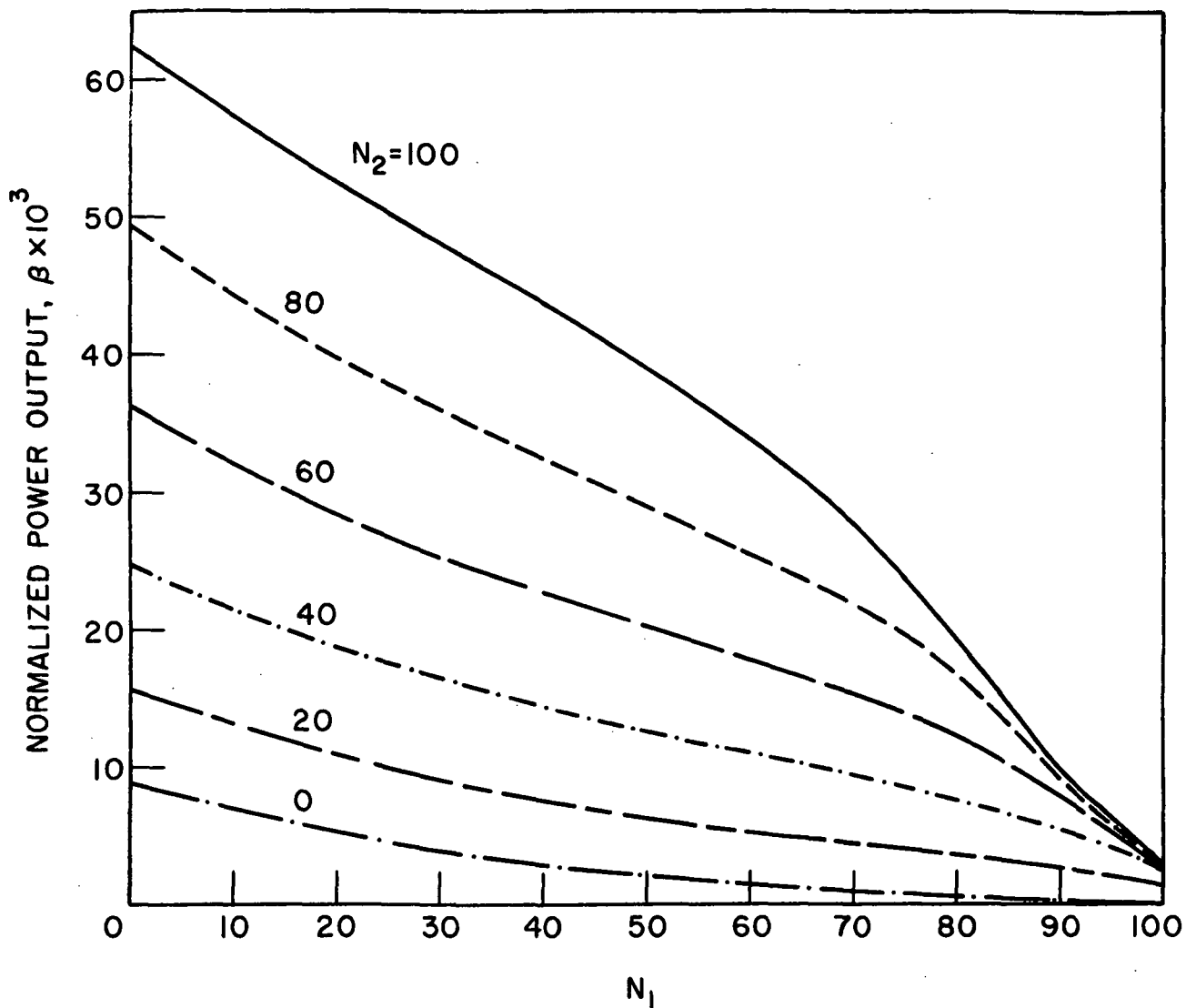


FIG. 5.4 THEORETICAL NORMALIZED POWER OUTPUT OF THE READ DIODE VARACTOR OF FIG. 5.1 FOR DIFFERENT N_1 AND N_2 VALUES. ($\gamma_1 = 0.5$, $\gamma_2 = 4$, $\bar{v}_{pt} = 0.2$, $\bar{v}'_{pt} = 0.3$, $\omega_{out}/\omega_c = 10^{-2}$)

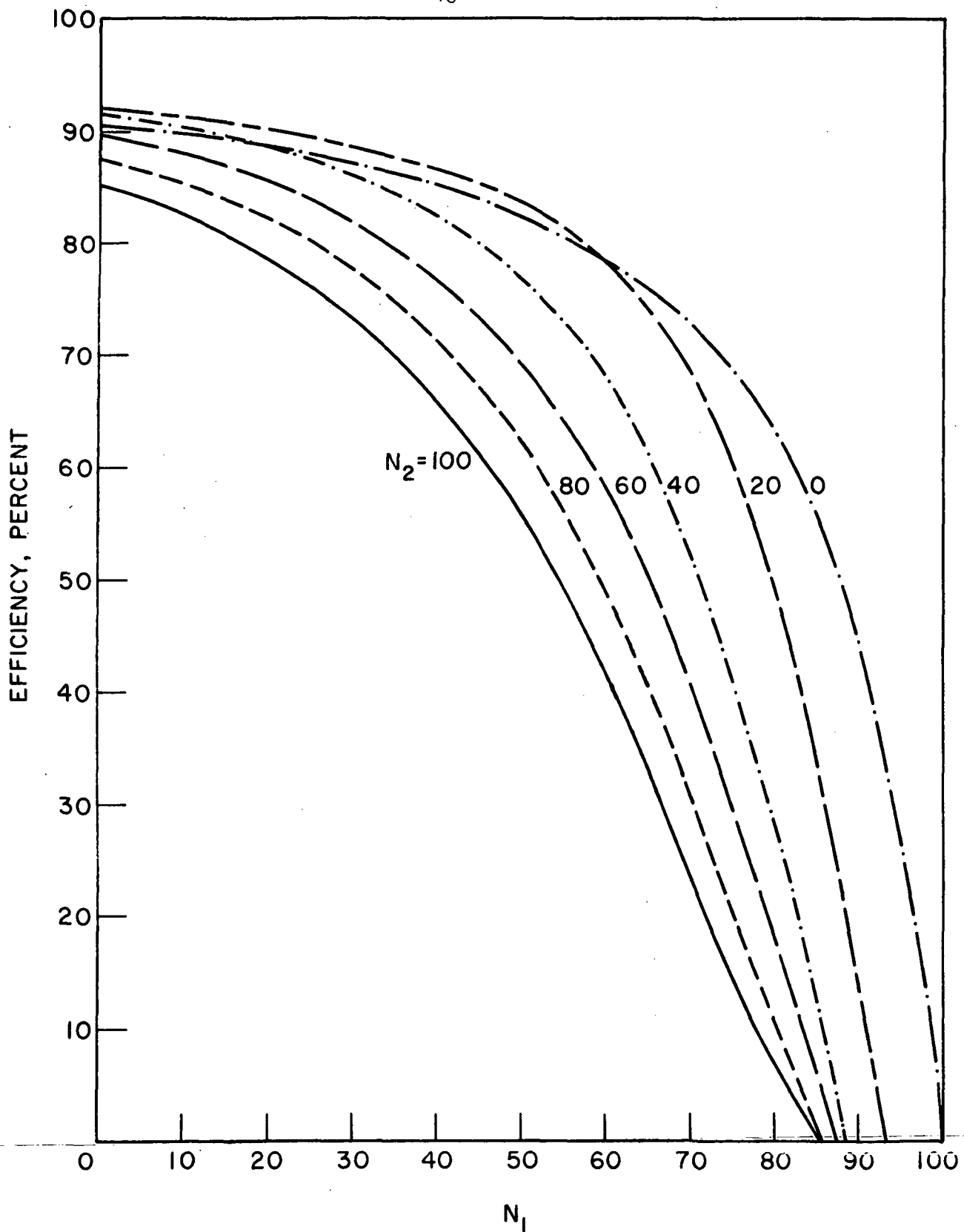


FIG. 5.5 THEORETICAL EFFICIENCY OF THE VARACTOR OF FIG. 5.2 FOR DIFFERENT N_1 AND N_2 VALUES. ($\gamma_1 = 0.5, \gamma_2 = 0, \bar{v}_{pt} = 0.2, \bar{v}'_{pt} = 0.2, \omega_{out}/\omega_c = 10^{-2}$)

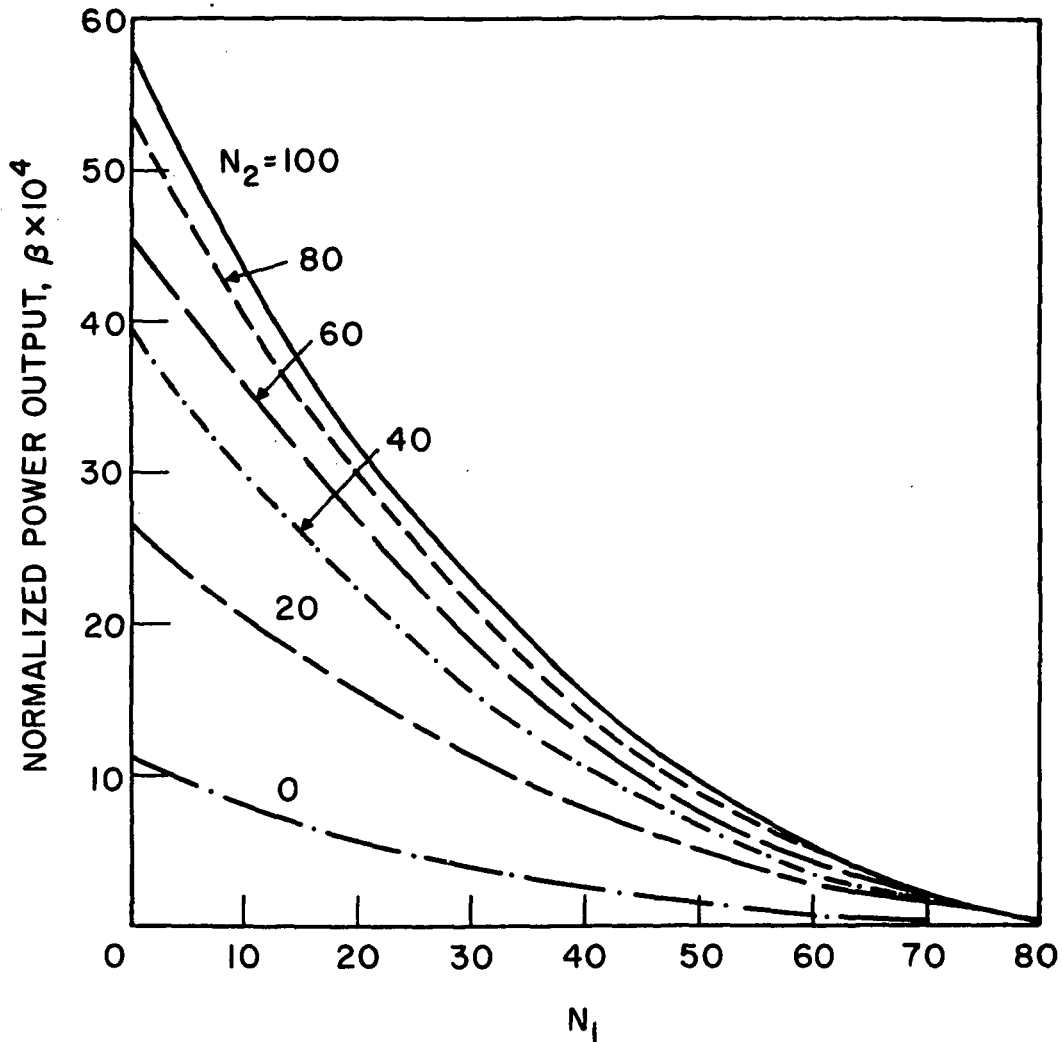


FIG. 5.6 THEORETICAL NORMALIZED POWER OUTPUT OF THE VARACTOR OF FIG. 5.2 FOR DIFFERENT N_1 AND N_2 VALUES. ($\gamma_1 = 0.5$, $\gamma_2 = 0$, $\bar{v}_{pt} = 0.2$, $\bar{v}'_{pt} = 0.2$, $\omega_{out}/\omega_c = 10^{-2}$)

5.3 Experimental and Theoretical C-V Characteristics of Read Diode Varactors. The theoretical formula of the C-V characteristic of the Read diode varactor when the i (intrinsic) layer is not purely intrinsic but contains some residual doping density defined as $n_d' = n_d(1 + \alpha)$ is not presented here. However, the theoretical calculation based on the data of the three-layer epitaxially grown Read diode made by Texas Instruments, Inc., type Read II, is presented in Fig. 5.7. The experimental results presented in Fig. 5.8 indicate good agreement between the two figures.

The theoretical C-V curves of a hypothetical Read diode having different doping densities in the i-region are presented in Fig. 5.9. This figure shows that the C-V characteristic of a Read diode can be appreciably changed by changing the doping density of the i-layer.

5.4 Conclusions. By comparing the performance of the Read diode varactor and that of a punch-through varactor, it can be concluded that the Read diode varactor has great potential as a small-signal harmonic generator with increased power output as well as high efficiency. Also, at large-signal operation it has definite advantages over other kinds of varactors with regard to power output, although the efficiency is not as high. The main drawback of the Read diode varactor for operation at high frequencies may result from decreased cutoff frequency because of the comparatively higher series resistance R_s , but the decreased value of C_{min} may nullify this effect considerably. All of these aspects will be studied experimentally.

5.5 Program for the Next Period. Effort will be continued to measure the quality factor Q of a Read diode varactor made by Texas Instruments, Inc., type Read II, in order to estimate the cutoff frequency. This

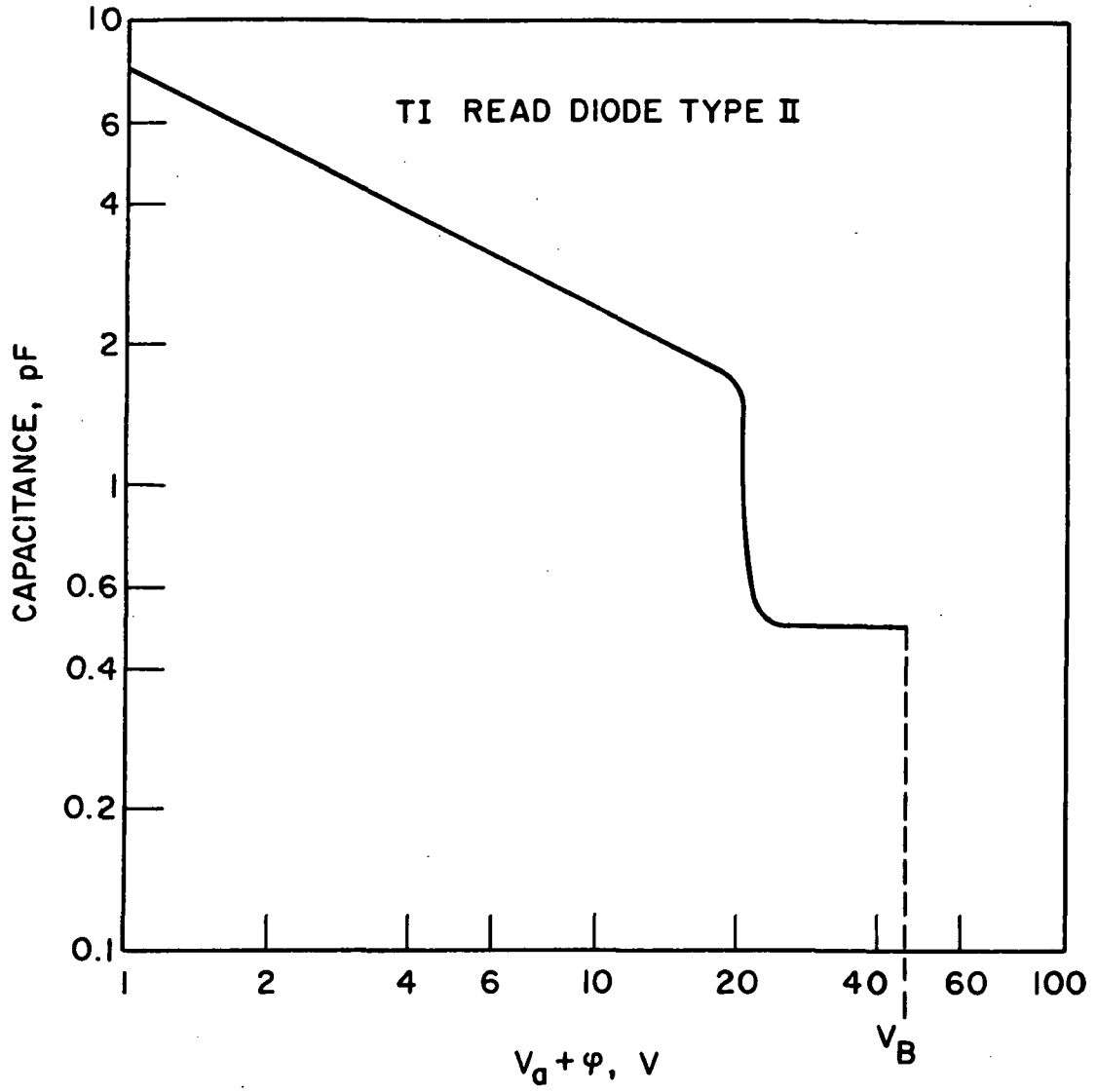


FIG. 5.7 THEORETICAL C-V CURVE OF THE TI READ DIODE.

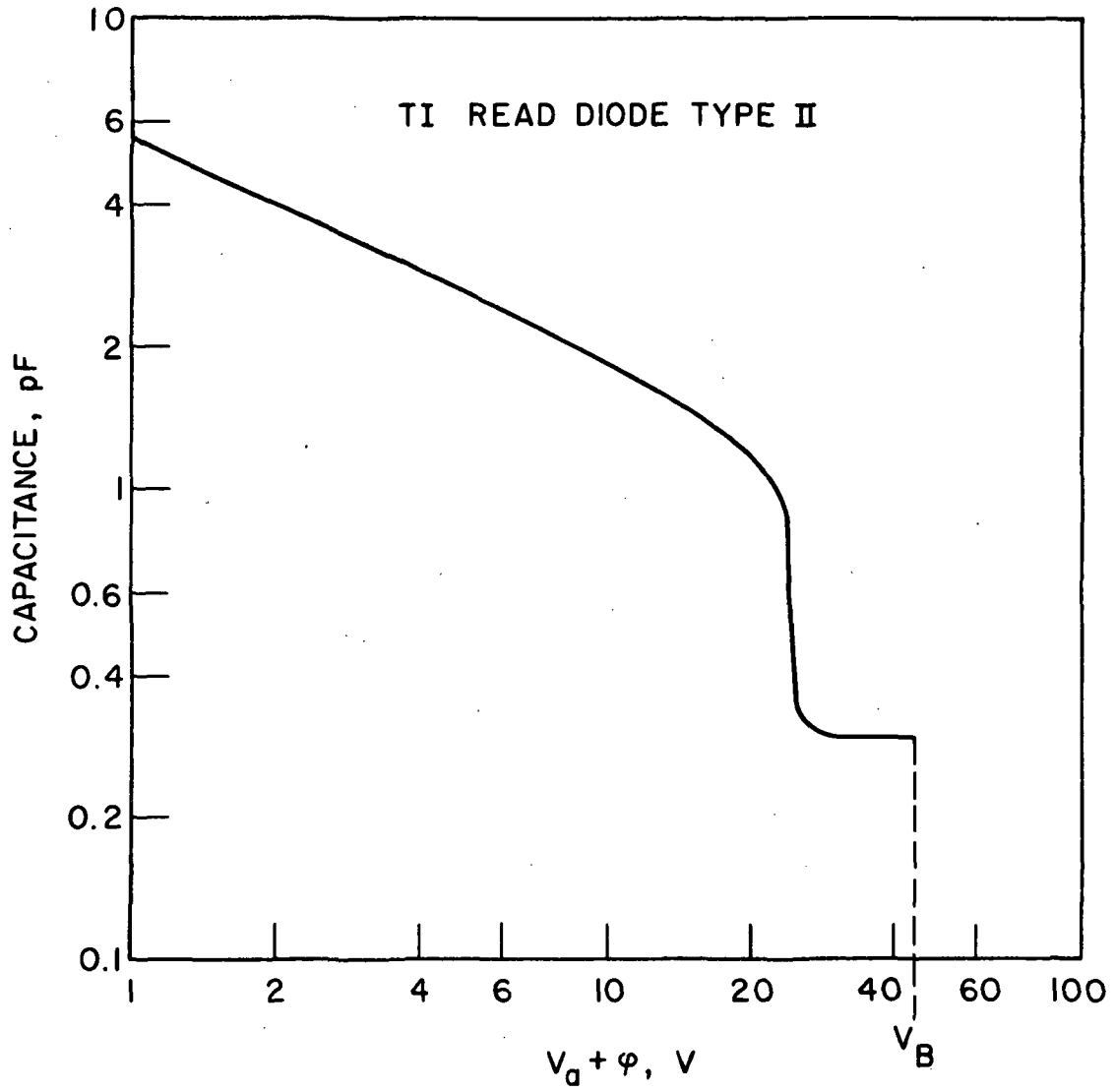


FIG. 5.8 EXPERIMENTAL C-V CURVE OF THE TI READ DIODE.

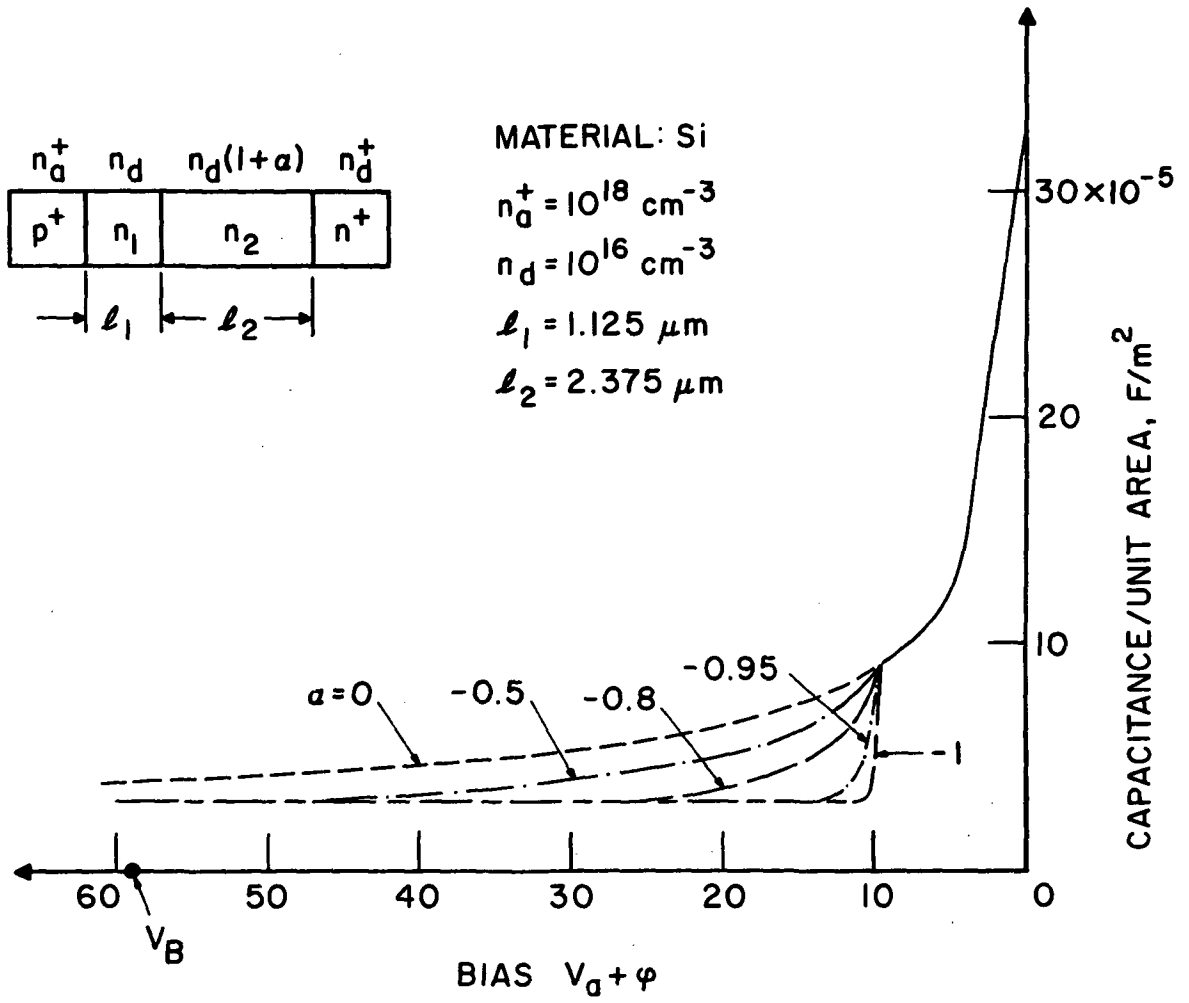


FIG. 5.9 THEORETICAL C-V CURVE OF A READ DIODE WITH DIFFERENT DOPING DENSITY IN THE i-LAYER.

information will be used to design a second-harmonic converter to determine how the theoretically predicted power output and efficiency agree with the experimental results.

6. Fabrication of Schottky-Barrier IMPATT Diodes

Supervisors: G. I. Haddad and S. N. Shabde

Staff: S. P. Kwok

6.1 Introduction. It was shown theoretically¹ that the effective avalanche width of a Si IMPATT diode using an n^+pp^+ structure is smaller than the corresponding complementary p^+nn^+ one. However, the problem of minority carrier storage² becomes increasingly more significant in a diode with a narrow avalanche region. A Schottky-barrier IMPATT diode using p-type Si could have the advantage of a narrow avalanche region without the minority carrier storage problem. During this period titanium (Ti) was used for the fabrication of Schottky barriers on a p-type Si wafer and the barrier height was determined. Meanwhile, the fabrication of a PtSi-Si(n) Schottky barrier also progressed considerably.

6.2 Ti-Si(p) Schottky Barrier.

6.2.1 Fabrication. A pp^+ Si wafer with a 2 Ω -cm and 3.5 μm thick epitaxial layer is first chemically thinned on the substrate side to approximately 0.001 inch. The wafer is then cleaned in TCE, acetone, Freon, HF and DI water. It is then prebaked in vacuum at 300°C for one-half hour and is allowed to cool for the same period. Then Ti (250 Å),

1. Schroeder, W. E. and Haddad, G. I., "Avalanche Region Width in Various Structures of IMPATT Diodes," Proc. IEEE (Correspondence), vol. 59, No. 8, pp. 1245-1248, August 1971.

2. Misawa, T., "Minority Carrier Storage and Oscillation Efficiency in Read Diodes," Solid-State Electronics, vol. 13, No. 10, pp. 1369-1374, October 1970.

Cr (250 Å) and Au (0.5 μm) are sequentially evaporated on the epitaxial layer. Cr and Au layers of the same thickness are used for making ohmic contact on the substrate side. Using the usual photolithographic technique diodes are formed and separated. To avoid sharp curvature in the junction due to undercutting during the etching process, the etching was done from the substrate side. A mixture of HNO₃ and HF (95%:5%) was found to be a mild enough etchant so as not to cause a severe undercutting of the Ti layer during Si etching. After the diodes have been separated they are ready for measurement.

6.2.2 Height of Ti-Si(p) Schottky Barrier. The I-V characteristic of a typical diode is shown in Fig. 6.1 and its C-V characteristics, in Fig. 6.2. The rise in capacitance value at high voltages is due to the high reverse saturation current. The slope of $1/C^2$ vs. voltage is constant at low voltages up to approximately 3 V. From the slope the acceptor impurity density of $7.4 \times 10^{15}/\text{cm}^3$ was obtained which corresponds to the specified resistivity of 2 Ω-cm. The height of the barrier was determined from the zero-volt intercept of the extrapolated forward current. The barrier height ϕ_{Bp} is given by the following equation:³

$$\phi_{Bp} = \frac{kT}{q} \ln \left(\frac{A^{**} T^2}{J_s} \right), \quad (6.1)$$

where k = the Boltzmann constant,

T = the temperature,

q = the electronic charge,

J_s = the zero-volt current intercept or the saturation current and

A^{**} = the Richardson constant.

3. Sze, S. M., Physics of Semiconductor Devices, John Wiley and Sons., Inc., New York, Chap. 8, 1969.

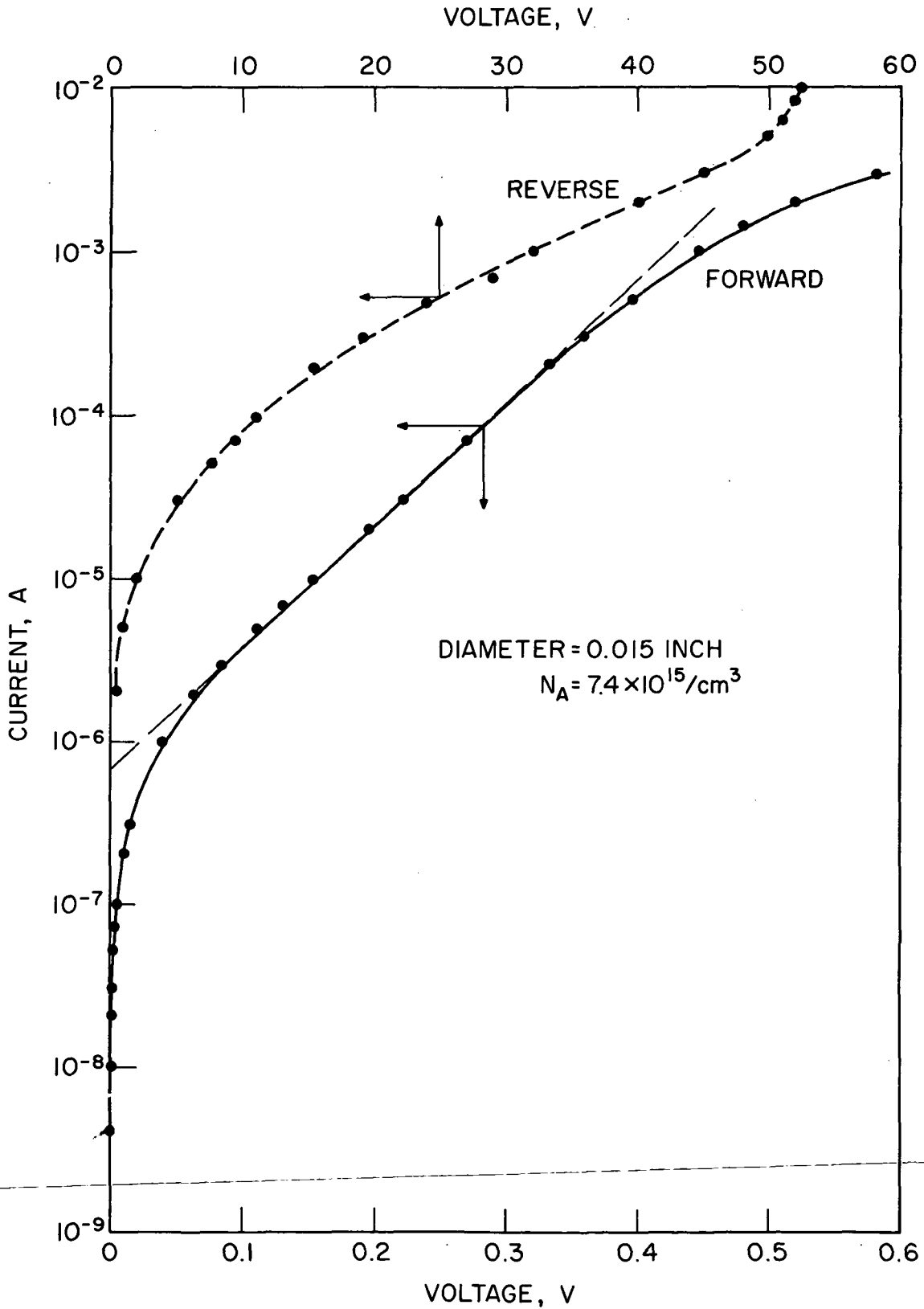


FIG. 6.1 I-V CHARACTERISTICS OF THE Ti-Si(p) SCHOTTKY BARRIER.

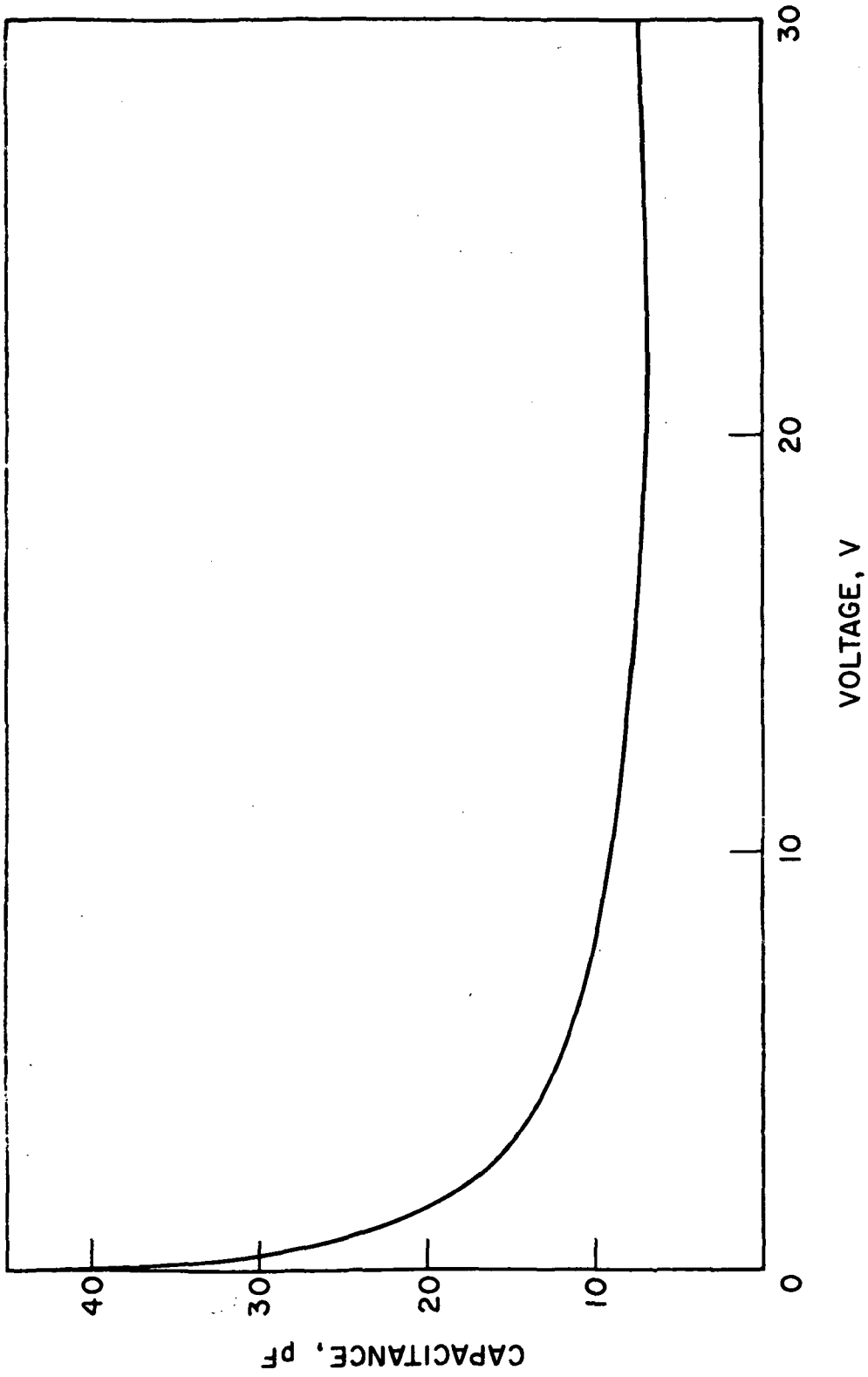


FIG. 6.2 C-V CHARACTERISTIC OF THE TI-SI (p) SCHOTTKY BARRIER.

The Richardson constant is taken to be $32 \text{ A/cm}^2/\text{K}^2$ for holes.³ This procedure yields $\phi_{\text{Bp}} = 0.58 \text{ V}$. The barrier height is calculated to be $\phi_{\text{Bp}} = 0.56 \text{ V}$ from the reverse current value at $1 \text{ V} \gg kT/q$ and the following expression:

$$\phi_{\text{Bp}} = \Delta\phi + \frac{kT}{q} \ln \left(\frac{A^{**} T^2}{J_s} \right), \quad (6.2)$$

where $\Delta\phi$ is the barrier lowering due to the image force, which is

$$\Delta\phi = \left(\frac{qE_m}{4\pi\epsilon} \right)^{1/2}, \quad (6.3)$$

E_m is the maximum value of the electric field and ϵ is the dielectric constant of the semiconductor.

On the other hand, the barrier height is related to the intercept of the $1/C^2$ line on the voltage axis, which is V_i , as

$$\phi_{\text{Bp}} = V_i + V_p - \Delta\phi + \frac{kT}{q}, \quad (6.4)$$

where

$$V_p = \frac{kT}{q} \ln \left(\frac{N_v}{N_A} \right), \quad (6.5)$$

N_v is the well-known effective density of states in the valence band and N_A is the acceptor impurity density taken to be $7.4 \times 10^{15}/\text{cm}^3$. The resultant ϕ_{Bp} is 0.60 V . Therefore it is concluded that the height of the Ti-Si(p) Schottky barrier is

$$\phi_{\text{Bp}} = 0.58 \pm 0.02 \text{ V} .$$

This value is higher than the highest barrier height of $ZrSi_2$ (0.53-0.55 V) reported recently.⁴

6.3 PtSi-Si(n) Schottky Barrier. A fabrication procedure for a PtSi-Si(n) barrier utilizing this laboratory's sputtering system has been established which yields good reverse breakdown characteristics as shown in Fig. 6.3. The figure shows a diode with background doping of $10^{16}/cm^3$, an epitaxial layer width of $3.5 \mu m$ and a breakdown of 65 V as expected theoretically. The basic steps of the fabrication are as follows:

1. Backsputter the wafer.
2. Heat the sputtering source and its surroundings for a few minutes and cool it by lowering the dc sputtering current. This step reduces the outgassing of the impurities during the subsequent sputtering.
3. Sputter Pt at a suitable rate of deposition.
4. Sinter the wafer in vacuum at approximately $650^\circ C$ for 5 to 10 minutes to form a platinum silicide interface.
5. Evaporate Cr and Au for ohmic contacts.
6. Separate the diodes. This may involve an additional etching of a thin Pt layer which remains there after sintering: this is done by using hot H_2SO_4 ($150^\circ C$) or aqua regia.

6.4 Conclusions and Program for the Next Period. The barrier height of Ti-Si(p) reported here was higher than the highest value of $ZrSi_2$ (p) reported elsewhere.⁴ However, a Schottky-barrier height of 0.58 V is still low for the application of IMPATT oscillators due to the inherent large reverse saturation current and its thermal instability. Most recently, hafnium-Si(p) Schottky barriers have been reported⁵ to have a

-
4. Andrews, J. M. and Lepselter, M. P., "Metal-Silicide Schottky Diodes," Solid-State Electronics, vol. 13, No. 7, pp. 1011-1023, July 1970.
 5. Saxena, A. N., "Hafnium-Si Schottky Barriers: Large Barrier Height on p-Type Si and Ohmic Behavior on n-Type Si," Appl. Phys. Letters, vol. 19, No. 3, pp. 71-73, 1 August 1971.

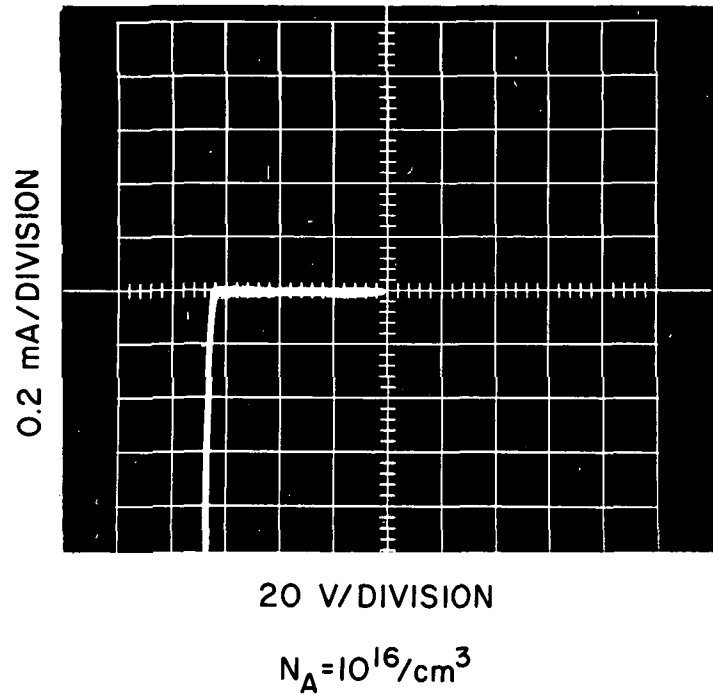


FIG. 6.3 BREAKDOWN CHARACTERISTIC OF A PtSi-Si(n) SCHOTTKY BARRIER.

height of 0.9 eV. The fabrication of an IMPATT diode using such a barrier will be pursued during the next period.

With the fabrication procedure of a PtSi-Si(n) barrier already successfully established, it is expected that X-band Schottky-barrier oscillators will be fabricated during the next period.